Prevailing Conditions for Dynamic Triggering in Intraplate and Plate-boundary Regions of the USA

Vivian Tang[1], Kevin Chao[1,2], and Suzan van der Lee[1,2,3]

[1]Department of Earth and Planetary Sciences, Northwestern University, Evanston, IL 60208

[2] Northwestern Institute on Complex Systems (NICO), Northwestern University, Evanston, IL 60208

3 Center for Interdisciplinary Exploration and Research in Astrophysics (CIERA), Northwestern University, Evanston, IL 60208

Corresponding author: Vivian Tang; Department of Earth and Planetary Sciences, Northwestern University, Evanston, IL 60208; Phone: +1-847-467-2467; Email: vivian@earth.northwestern.edu

Abstract

To facilitate identification of conditions that lead to the dynamic triggering of seismic events as catalogs of these events keep growing, we applied a machine-learning algorithm (decision tree) to a published data set of known instances of dynamically triggered seismic tremor in central California. To investigate the possible universality of our findings and to further test the algorithm, we also applied it to new observations, presented here, of potentially dynamically triggered seismic activity in three intraplate regions: Raton Basin (CO), Yellowstone, and central Utah. We report potential tremor or local earthquake signals from here during the propagation of surface waves from the 2012 M_w 8.6 Sumatra earthquake. These surface waves also triggered seismic activity along the western boundary of the North

American plate and did not trigger seismic activity in the central and eastern USA. We report additional potential dynamic triggering in the three aforementioned intraplate regions from an investigation of seismograms from 37 additional large earthquakes, recorded between 2004 to 2017.

Our findings show that transient stresses generated by surface waves from large earthquakes and arriving from favorable directions generally lead to triggered tremor in seismically, volcanically, and hydrothermally active regions like central California and possibly Yellowstone. These stresses do not appear to be decisive factors for the potentially dynamically triggered local earthquakes reported for the Raton Basin and central Utah, while surface waves' incidence angles do appear to be important there.

Key Points:

1. New detections of possible dynamically triggered tremor and earthquakes in Yellowstone, Utah, and the Raton Basin, Colorado.
2. For local earthquake triggering peak stress is *not* decisive while for triggering tremor it needs to exceed a threshold.
3. Machine learning and visualization identify surface waves' incidence angles as an important factor for dynamic triggering.

1. Introduction

Far-field surface waves of large magnitude earthquakes can dynamically trigger seismic events such as small, local earthquakes (*Prejean et al.*, 2004) and tectonic tremor (*Peng and Gomberg*, 2010). Figure 1 shows two examples of such events. Dynamic triggering of seismic

events has been reported for peak stress perturbation estimates of a mere 1 or 2 kPa, (*Peng and Gomberg*, 2010; *Brodsky and van der Elst*, 2014). As triggered seismic events might occur only while the cumulative stress at a fault approaches its pre-slip state, a quantitative observation of triggered seismic events may provide useful information on the state of stress on the fault (*Peng and Gomberg*, 2010; *Kato et al.*, 2013). Analyses of triggered seismic events also contribute information and insight on other factors that contribute to triggering and nucleation processes and mechanics in general.

Triggered tremor and triggered earthquakes have been observed at plate boundaries and major faulting systems world-wide. Along the western boundary of the North American Plate, many studies have reported dynamic triggering of local earthquakes (*Velasco et al.*, 2008; *Aiken and Peng*, 2014; *Brodsky and van der Elst*, 2014; *Hill and Prejean*, 2015) and tectonic tremor (*Gomberg et al.*, 2008; *Peng et al.*, 2009; *Rubinstein et al.*, 2009; *Chao et al.*, 2012; *Gomberg and Prejean*, 2013; *Aiken and Peng*, 2014; *Chao et al.,* 2017). Fewer studies reported triggered seismic events in the continental interior of the United States (*Prejean et al.*, 2004; *Freed*, 2005; *Van der Elst et al.*, 2013; *Velasco et al.*, 2016). Within the intraplate interior of North America, the geothermally, volcanically, and seismically active region around Yellowstone National Park experienced dynamic triggering following the 2002 Denali earthquake (*Husen et al.*, 2004), as did the Wasatch Fault zone in Utah (*Pankow et al.*, 2004). Van der Elst et al. (2013) report delayed dynamic triggering of local earthquakes in regions of anthropogenic seismicity such as the Raton Basin, Oklahoma, and Snyder, Texas, for three days following the 2011 M_w 9.1 Tohoku, the 2010 M_w 8.8 Chile earthquakes. Velasco et al. (2016) also found triggered earthquakes in Texas as well as the Coso region in California, respectively, following the same two earthquakes. Velasco et al. (2016) expanded their search

by using an automatic approach for detecting triggered seismicity in the conterminous United States with USArray, as did Cerda et al. (2011) and Linville et al. (2014), for example. Machine-learning algorithms can also expand event searches to cover bigger data sets (*Ramirez and Meyer*, 2011; *Lecun et al.*, 2015; *Tang et al.*, 2020). The number of dynamically triggered events reported in the literature keeps growing (*Canitano et al.,* 2019), suggesting that their quantity and pervasiveness can be expanded and exploited to study the conditions necessary for such triggering in a new, scalable manner.

In this study, we expand the diversity of reported dynamically triggered seismicity by exploring additional activity in the continental, intraplate interior of the United States and we show that a decision-tree machine-learning algorithm is well suited for determining the conditions that prevail during dynamic triggering from ever increasing catalogs of triggered events. To do the former we first interactively investigated all broadband seismograms of the 2012 M_w 8.6 Sumatra earthquake recorded in the USA. Secondly, we investigated seismograms of thirty-eight $M_w > 7$ earthquakes recorded in three intraplate regions found in step one to contain signals from triggered seismicity in records of the 2012 M_w 8.6 Sumatra earthquake. To investigate the ability of a machine-learning algorithm to identify prevailing conditions during dynamic triggering, we introduce and apply a decision-tree algorithm to our new observations of intraplate dynamic triggering, as well as to a known dataset of triggered tremor in California (*Chao et al.*, 2012). Finally, we discuss to what extent peak dynamic stress estimates, as well as other attributes, are decisive factors for triggering tremor and/or earthquakes.

2. Data mining for potentially triggered seismic events: Data and Methods

2.1 The 2012 M_w 8.6 Sumatra earthquake

The 11 April 2012 M_w8.6 Sumatra earthquake is the largest magnitude strike-slip earthquake recorded to date (*Meng et al.*, 2012) and it radiated large-amplitude Love waves with one of four radiation maxima oriented towards USArray (*Rösler and Van der Lee*, 2020). As Love waves hold considerable dynamic triggering potential (*Peng and Gomberg*, 2010; *Hill*, 2012; *Bansal et al.*, 2016, 2018; *Chao and Obara*, 2016; *Johnson and Bürgmann*, 2016; *Kundu et al.*, 2016; *Chao and Yu*, 2018; *Castro et al.*, 2015), we searched for signals in USArray and other US data from potentially dynamically triggered intraplate seismic events that occurred during the passage of surface waves from the 11 April 2012 M_w 8.6 Sumatra earthquake. Love waves can temporarily enhance shear stress on faults they propagate across. Van der Elst et al. (2013) examined dynamic triggering by this earthquake's surface waves in regions of anthropogenic seismicity and in two locations found an elevated number of local earthquakes during post-teleseismic-earthquake days. However, this elevated number was much smaller than that found following the 2011 M_w 9.1 Tohoku, the 2010 M_w 8.8 Chile earthquakes, which had stronger Rayleigh waves. It may be unlikely that Love waves are a primary cause of triggering seismic activity in regions with little tectonic activity. Here we are interested in the possible triggering of tectonic events and choose the 2012 M_w 8.6 Sumatra earthquake, with its high-amplitude Love waves, to begin testing of this hypothesis.

2.2 USArray data processing

During the 2012 M_w8.6 Sumatra earthquake all seismic components of EarthScope's USArray (http://www.usarray.org) were in place: The Transportable Array (TA), the Flexible Array (FA), the Reference Network, as well as cooperating regional networks such as the

University of Utah Regional Seismic Network (UU). The TA has been operating since 2004, migrating from west to east across the United States at a snail's pace before leaping to Alaska, where it is currently deployed. The TA, equipped with three-component broadband stations separated by an approximate 70 km, is a large-scale seismic network. The FA consists of similar broadband stations that were deployed in smaller regions in more flexible geometries for limited durations by individual research teams. Here we included data from USArray and other permanent and temporary seismic networks, such as the ANSS, that were recording in the USA during the first greater decade (hereafter called a dodecade) of EarthScope (See "*Acknowledgements and Data*" for details).

For the 2012 M_w 8.6 Sumatra earthquake, we downloaded all available broadband seismograms recorded in the USA via IRIS DS (Incorporated Research Institutions for Seismology, Data Services) (see "*Acknowledgements and Data*" for details). The downloaded waveforms start 60 minutes before and end 180 minutes after the origin times of the earthquake. The waveforms were loaded into and examined in CrazyTremor (section 2.4) in different frequency bands. The waveforms were filtered with a 2-8 Hz band-pass filter when searching for triggered tremor and triggered earthquakes. Frequency content above 8 Hz is not available or reliable for all stations, which have different instrumentation and sampling rates. Waveforms without high-frequency signals from local earthquakes or tremor were removed. The remaining waveforms were converted to ground velocity, by deconvolving with the instrument response.

2.3 Criteria for identifying triggered tremor and triggered earthquakes

Signals from triggered earthquakes are similar to signals from small local earthquakes and have visible *P* and *S* wave energy at frequencies above 5 Hz. To identify *P* and *S* waves, we examined three-component seismograms. In this paper, earthquake signals are only considered as potentially triggered when they occur during the propagation of the surface wave train and have a statistical probability of occurring during that time window of 3% or less. We consider an earthquake as possibly triggered (*Aiken and Peng*, 2014) if: (1) the earthquake occurs during the propagation of Love and Rayleigh wave trains, (2) the earthquake signal has elevated power within the passband between 2 and 8 Hz; (3) the earthquake signal shows clear *P*- and *S*-waves (Figure 1b); (4) the signals come from local earthquakes rather than teleseismic aftershocks, (5) there is little to no local activity within 24 hours before the examined time window.

Bursts of triggered tremor occur during surface wave trains and can last for 5 to 30 minutes. To identify possibly triggered tremor, we use the following criteria (*Chao and Yu*, 2018): (1) tremor occurs during the propagation of Love and Rayleigh wave trains, (2) tremor has dominant frequencies between 2 and 8 Hz; (3) tremor looks like a series of bursts, with a similar modulating frequency as that of the coeval surface waves (Figure 1a); (4) the tremor is either recorded by at least two stations within a 50 km of epicentral distance (*Chao et al.*, 2019) or has been activated by more than one large teleseismic earthquakes.

2.4 Initial identification with CrazyTremor

Initial separation of waveforms with signals that meet the criteria outlined in section 2.3 from those without such signals was carried out through visual inspection using CrazyTremor (*Chao and Yu*, 2018), which was developed specifically to facilitate finding dynamically

triggered tremor and earthquakes. After loading SAC files into the CrazyTremor GUI (Figure 2), all seismograms were filtered (2-8 Hz band-passed) and compared with surface waves in the broad-band seismogram. The three components of each seismograms were examined at the same time and viewed as time series, envelopes, and/or spectrograms, to assist in the identification of stations with triggered signals. Next, we used the tagging function of CrazyTremor to reject stations with no signals from triggered events and only kept stations with signals of potentially triggered events. Finally, we sorted the filtered seismograms by increasing distance from the teleseismic earthquake, to confirm that the identified signals came from a local event rather than the sane source area as the teleseismic earthquake.

2.5 Earthquakes Investigated

In addition to interactively examining seismograms of the 2012 M_w 8.6 Sumatra earthquake (Figure 3) from over one thousand seismic stations, we examined seismograms from a subset of stations for 37 additional earthquakes with $M_w > 7.0$ (Table 1), and one, slightly smaller foreshock. The subsets of stations were selected to be in three intraplate regions where surface waves from the 2012 M_w 8.6 Sumatra earthquake possibly triggered tremor or a local earthquake. The selected earthquakes not only had moment magnitudes (M_w) greater than 7.0, they also had event depths less than 100 km, and were at least 10° away (*Chao and Obara*, 2016) from the investigated station locations. Between 2004 and 2017, 175 earthquakes matched these criteria. For each location, we estimated the surface wave amplitudes generated by the large earthquake's surface waves using a magnitude-distance relationship (*Chao et al.*, 2013), and rejected earthquakes with estimated ground velocity

amplitudes below 0.1 *mm/s*. We use the ground velocity to estimate the associated change in shear stress σ as

$$\sigma = \mu \dot{u}/U$$

, where μ is the shear modulus, $\dot{u}$ is the surface-wave ground velocity, U is the surface wave's group velocity, and $\dot{u}/U$ approximates half the deviatoric strain, (*Chao and Obara*, 2016). Using μ = 35 GPa as a representative shear modulus for the crust and U = 3.5 km/s as a representative average group velocity, we estimate the peak shear stress in kPa to equal $10^4 \times A$, where A is the ground velocity in m/s. This implies that the 37 additional earthquakes we selected (Figure 4) were estimated to cause dynamic stress changes that exceeded 1 kPa. We then investigated whether these earthquakes' surface waves triggered seismicity in the three identified locations. We list all selected earthquakes in Table 1 and number them for easy reference. The 2012 Sumatra earthquake is earthquake #21. Earthquake #30 had a smaller M_w 6.5 foreshock (not listed in Table 1) whose surface waves also potentially triggered a local earthquake in central Utah.

3. Data mining for potentially triggered seismic events: Results

3.1 Observations of potentially triggered seismic events following the 2012 M_w 8.6 Sumatra earthquake: Overview and western plate boundary

After visual examination in CrazyTremor (*Chao and Yu*, 2018) of radial, transverse and vertical components of 1,021 seismograms of the 2012 Sumatra earthquake (Figure 3), we rejected 617 seismograms because they exhibited either no high-frequency energy in the surface wave window or contained data gaps, calibrations, mass centerings, instrument- or site-specific signals, or other non-tectonic signals (*Marcillo and McCarthy*, 2020). Next, we

visually inspected the surface-wave windows in the remaining 404 candidate seismograms for this earthquake in one or more frequency bands (i.e., 2-8 Hz band-pass or 5 Hz high-pass filter), using Seismic Analysis Code (SAC) (*Goldstein et al.*, 2005). We identified signals as from local earthquakes or from tremor if they met the pertinent criteria outlined in the previous section. Of these 404 seismograms, 47 candidates had signals that met the criteria for being from potentially dynamically triggered events. The rest of the seismograms contained some type of high-frequency signal or noise in the surface window that neither qualified as a tremor nor as an earthquake signal. Thirty-six out of these 47 candidates were observed along the western plate boundary (Figure 3, Table S1), where triggered events had previously been observed for other teleseismic earthquakes (*Peng et al.*, 2009; *Chao et al., 2012*; *Castro et al.*, 2015 and *Castro et al.*, 2017).

3.2 Intraplate triggering following the 2012 M_w 8.6 Sumatra earthquake: western USA

From detailed inspections of the remaining eleven candidates for newly discovered dynamic triggering east of the plate boundary, we rejected a further five. These rejections are based on instrument- or site-specific noise, including frequent occurrence of similar signals before and after the surface wave window in regions that are seismically relatively quiescent. One of the six remaining signals represents a possibly dynamically triggered local earthquake (Figure 3) in central Utah (station SRU).

Four of the six signals represent a dynamically triggered earthquake (Figure 3) in Colorado (stations SDCO, T25A, Q24A, and S22A). Van der Elst et al. (2013) included this detection at station T25A in his three-day catalog of seismicity that followed the 11 April 2012 M_w 8.6 Sumatra earthquake. Because of its longer deployment, we selected SDCO as a

representative station for searching for dynamically triggered earthquakes during surface wave trains from additional large earthquakes (section 3.4).

The final one of the six remaining signals possibly represents dynamically triggered tremor (Figure 3) in Yellowstone (station H17A). However, several signals with comparable time progressions and bandwidth were recorded by the station in the hours leading up to the Sumatra earthquake, while other stations about 10-20 km north of H17A did not record the signal, suggesting a possibly shallow source. In addition to being tectonically active, Yellowstone is also volcanically and hydrothermally active (*Huang et al.*, 2015, *Vandemeulebrouck et al.,* 2013; *Hurwitz et al.,* 2014). Station H17A is located within the Yellowstone Caldera.

3.3 Absence of triggering following the 2012 M_w 8.6 Sumatra earthquake: Central and Eastern USA

The seismograms of the 2012 Sumatra earthquake that we examined were recorded at a dense collection of seismic stations (Figure 3), including a Midwestern swath of TA and FA stations. At this time, the largest distance between two neighboring stations in the USA, away from TA and FA stations, was around 200 km. Each seismogram recorded in the central and eastern USA (CEUS) was inspected in different frequency bands, and all were rejected as not having recorded dynamically triggered seismicity. Likewise, Van der Elst et al. (2013) examined dynamic triggering by this earthquake's surface waves in regions of anthropogenic seismicity and found virtually no triggering in the CEUS, including at sites of anthropogenic seismicity in Texas, Arkansas, and Ohio. However, they did find a moderate surge in seismic activity in a wastewater injection area in Oklahoma (near stations V34A and V35A) and in

Colorado (near stations SDCO and T25A) during the days that followed the Sumatra earthquake. *Bockholt et al*. (2014) report finding neither ambient nor triggered tremor around the Reelfoot Fault in northern Tennessee during surface wave propagation from 11 large additional earthquakes. Our analysis further confirms the absence of dynamic triggering of tectonic seismic activity across all of the CEUS during the passage of surface waves from the 2012 M_w 8.6 Sumatra earthquake.

3.4 Observations of potential dynamic triggering following 37 additional large earthquakes.

We examined seismograms recorded at the three intraplate locations represented by stations H17A, SRU, and SDCO, from 37 additional large earthquakes (see section 2.5). With some of these earthquakes being recorded by a subset of the stations (H17A, SRU, and SDCO), we obtained 97 additional seismograms to examine. Within these 97 seismograms and for 7 of the 38 earthquakes in total, we found possible dynamically triggered events recorded within the surface-wave arrival window (Figures S2-S9). We also examined seismograms at nearby stations for each newly found potentially triggered event. Using observations of the same local events at nearby stations and through picking *P* and *S* wave arrival times in CrazyTremor, we were able to locate 8 local events (Figure 5). We estimated peak dynamic shear stress from the vertical- and transverse-component ground-velocity seismograms of all 38 earthquakes and plotted them versus back-azimuth in Figure 6. In the following sub-sections, we discuss these new detections (Figures 7 and 8) in detail for each of the three intraplate locations.

3.5 Observations of triggered tremor in Yellowstone (H17A station)

Station H17A station in Yellowstone National Park recorded tremor signals potentially triggered by four of the 28 earthquakes for which H17A data were available (Table 3): #20 (Figure 1), #21 (Figure 3), #12 (Figure S1), and #37 (Figure S2). The tremor signals for earthquake #20 (20 March 2012 M_w7.5 Mexico) are clear. No tremor-like signals occur within several hours before and after the surface wave window. Tremor signals detected in the surface wave windows of earthquakes #12, #21, and #37 *are* accompanied by comparable tremor-like signals in several hours before and after the windows. Moreover, the tremor signals were not recorded by stations 10-20 km north of H17A, suggesting a shallow, relatively local and possibly non-tectonic source for the tremor. Peak dynamic stresses estimated from H17A's vertical- and transverse-component recordings of the surface waves from earthquake #20 are above 20 kPa, as is also the case for earthquake #37 and two earthquakes that did not trigger tremor in Yellowstone. The majority of the 24 recorded, non-triggering earthquakes produced peak dynamic stress estimates under 10 kPa. Figure 6 shows that surface waves from all four earthquakes arrived from either the NW or the SE, while non-triggering surface waves arrived from these and additional SE azimuths. Estimated peak stresses and other attributes for H17A are provided in Table S2 for all earthquakes.

3.6 Observations of triggered earthquakes in central Utah (SRU station)

Station SRU in central Utah recorded 34 of the 38 examined earthquakes and its seismograms show signals of local earthquakes that were potentially triggered by surface waves from the following seven large earthquakes (Table 4): #21 (Figure 3), #24 (Figure S7), #8 (Figure S3), #9 (Figure S4), #10 (Figure S5), #13 (Figure S6), and #30 (Figure S8). Interestingly, peak dynamic stresses inferred from these SRU recordings do not differ

297 substantially from the distribution of peak dynamic stresses inferred from non-triggering
298 teleseismic earthquakes.

299 We searched for potentially triggered local earthquake signals in seismograms from
300 earthquake #21 (Figure 7) recorded at stations within about 100 km from SRU station (Table 4).
301 We observed signals from this local earthquake at seven nearby stations: TMU, CVRU, BCE,
302 PNSU, ROA, DCM and ARGU, and located its epicenter (Figure 5) using CrazyTremor. Like
303 those from #21, surface waves from earthquake #24 also triggered a local earthquake in the
304 Raton Basin (see next section). At the time of earthquake #24, noise levels at H17A
305 (Yellowstone) were too high to detect triggered seismicity signals. The local, SRU-recorded
306 earthquake potentially triggered by earthquake #24 was also recorded by nearby stations
307 ARGU, DCM and PNSU. Also, during surface wave propagation from earthquakes #8, #9, #10,
308 and #13, signals that could be from local earthquakes were recorded at station SRU. However,
309 other earthquake signals and earthquake-like signals were recorded within hours before and
310 after the surface wave window. The local earthquake potentially triggered by earthquake #9
311 was recorded at SRU and 7 nearby stations (P14A, Q14A, P16A, Q16A, P17A, R17A and
312 Q18A) and we picked *P* and *S* wave arrivals in these 8 records to locate the epicenter of this
313 local earthquake (Figure 5). Potentially triggered earthquake signals were recorded at 7 nearby
314 stations (TMU, Q18A, Q16A, P18A, ROA, P17A, DBD) from earthquake #10. The local
315 earthquake potentially triggered by earthquake #13 occurs late w.r.t. the surface wave window.
316 We picked *P* and *S* wave arrivals at 14 nearby stations (stations SRU, Q16A, P18A, S18A,
317 P19A, O19A, DUG, Q20A, R20A, O20A, S20A, N20A, N21A, N22A and R24A) to locate the
318 epicenter of this local earthquake (Figure 5).

Earthquake #30 presents an interesting case as it may have triggered a local earthquake in central Utah not only during passage of surface waves from earthquake #30, but also, and with higher magnitudes, during the *S*-wave arrival and during the surface wave window for a M_w 6.5 foreshock, as well as 2 hours earlier and 3 hours later, yielding 5 local earthquakes in 6 hours of recording. The amplitudes of these earthquakes local earthquakes suggest that they have magnitudes roughly between 1.0 and 2.0. Background seismicity rates obtained from the USGS (earthquake.usgs.gov) in this part of central Utah, combined with the Gutenberg-Richter relationship between earthquake frequency and magnitude, suggests that there should be about 10 earthquakes with magnitudes between 1 and 2 per week. This rate translates to about one such earthquake per 18 hours, definitely raising our 5 earthquakes in 6 hours as anomalous, with three of these as possibly triggered by teleseismic earthquake #30 and its M_w 6.5 foreshock.

Station SRU is located at the San Rafael Swell (*Delaney and Gartner*, 1997) in central Utah, about 100 km east of a roughly north-south oriented belt of seismicity, the Levan segment of the Wasatch Fault, and about 50 km south of a more east-west oriented lineament of seismicity. Quarry blasts reported by the USGS predominantly occur in the northern part of Utah, more than 50 km from station SRU. However, SRU is about ~20 SE of the Cleveland-Lloyd Dinosaur Quarry, an excavation site and open-air museum for dinosaur fossils and therefore an unlikely site for strong or frequent blasts. The detected SRU signals typically have strong S waves and no preference for the time of day or night at which they occur, further arguing against an anthropogenic source for the signals. During the past 20 years, the USGS reported about 3000 earthquakes with magnitudes between 2.0 and 3.0 located within a 50-km radius from SRU, which translates to about one such earthquake per week.

Therefore, the odds of finding such an earthquake within a ~2000 s long surface wave train by chance are about 0.3 %, which translates to 3% for earthquakes with magnitudes comparable to the ones we detected ($1 < M_w < 2$). The strongest earthquake in this area had a magnitude of 4.2 during the dodecade spanned by our study (https://earthquake.usgs.gov/). Prior to this, earthquakes were reported to have been dynamically triggered on the Wasatch Fault by surface waves from the 2002 Denali fault earthquake (*Pankow et al.*, 2004).

3.7 Observations of triggered earthquakes in Colorado (SDCO station)

Three local earthquakes recorded by station SDCO in Colorado were potentially dynamically triggered, respectively, by teleseismic earthquakes: #21 (Figure 3), #23 (Figure S9) and #24 (Figure 1). Earthquakes #21 and #24 also appear to have triggered local earthquakes in central Utah. The inferred peak dynamic stresses for these recordings (Table S2), again do not differ substantially from the distribution of peak dynamic stresses inferred from surface waves that did not trigger a local earthquake.

Station SDCO is at the eastern edge of the Colorado Plateau and by the northern branch of the Rio Grande Rift. The region around SDCO is not particularly seismically active. The closest known earthquakes to SDCO are a pair of 2003 M~3 earthquakes, 25 km SE of the station (https://earthquake.usgs.gov/). However, the station is about 80 km northwest of the Raton Basin, which has experienced an increase in seismic activity and wastewater injection over the past two decades (*Nakai et al.*, 2017; *Yeck et al.*, 2016; *Van der Elst et al,.* 2013)

For earthquake #21, we observed potentially triggered earthquake signals at 7 nearby stations (SDCO, T25A, Q24A, S22A, XTOCO, HGTCO and LVTCO) and used them in CrazyTremor to locate the epicenter of this local earthquake (Figure 8).

For earthquake #21 (Figure 5), the local earthquake signals in Utah arrive about 5,430 seconds after the origin time of earthquake #21 while in Colorado they arrive about 200 seconds later, which indicates that the surface waves from earthquake #21 triggered a local earthquake earlier in Utah than in Colorado. Figure 3 shows that these surface waves propagated roughly from northwest to southeast in the western US and would have indeed needed about 200 s to travel from station SRU in Utah to station SDCO in Colorado. This evidence suggests that these earthquakes in Utah and Colorado are indeed dynamically triggered, by the same component of the wavefield, rather than coincident earthquakes.

Earthquake #23 produced the local earthquake signal with the largest amplitude and observed by the most nearby stations. It was observed at 17 stations (SDCO, T25A, S22A, Q24A, ANMO, TASL, TASM, KSCO, MVCO, ISCO, AMTX, MSTX, CBKS, OGNE, SRU, MNTX and WMOK). Using *P* and *S* wave picks in CrazyTremor we located the epicenter of this earthquake to be in the Raton Basin (Figure 5). The local earthquake potentially triggered by teleseismic earthquake #24 was observed only at SDCO with an order of magnitude lower amplitudes than for earthquake #23 and relatively late in the surface wave train.

4. Testing of triggering threshold with a decision-tree algorithm

4.1 Motivation

Despite searching systematically through 1) over a thousand continent-wide seismograms from one earthquake (#21) and 2) hundreds of seismograms recorded in three particularly interesting intraplate regions from the 38 largest earthquakes of the dodecade spanned by our study, we found little evidence for dynamic triggering of tectonic tremor and earthquakes. Even in the three intraplate regions where we did detect potentially triggered seismicity, there

388 are no obvious patterns as to when triggering occurs and when it does not. Meanwhile, our
389 study is not alone in attempts to detect intraplate triggering (*Velasco et al.*, 2008, *Bockholt et*
390 *al.*, 2014, *Van der Elst et al*., 2013, *Velasco et al.,* 2016) and detections of dynamically
391 triggered seismicity at plate boundaries continue to accumulate (*Canitano et al.*, 2019). In the
392 second part of this paper we therefore explore the benefits of utilizing a machine learning
393 algorithm to 1) help detect the prevailing conditions under which dynamic triggering occurs, 2)
394 formalize the process of inferring these conditions and quantify possible detection thresholds,
395 3) prepare for larger volumes of plate boundary data on dynamic triggering that might
396 overwhelm researchers, and 4) prepare for investigating a larger number of factors that may or
397 may not contribute to creating the conditions for triggering. We choose to do so with a decision
398 tree algorithm. This algorithm takes as input the attributes of all of our detections as well as the
399 labels that indicate whether dynamic triggering occurred or not. Even though we have referred
400 to our intraplate detections as being *potentially* dynamically triggered, for evaluating the
401 algorithm we assume that they were indeed dynamically triggered. As attributes we provide the
402 algorithm with values of familiar attributes, such as peak stress estimates from peak ground
403 velocity and information about solid-earth tides, as well as with time of the day, and back
404 azimuth patterns.
405
406 **4.2 Theory of decision-tree**
407 The decision tree is a machine-learning algorithm, which can also be used as a prediction
408 method once enough data are available (*Mitchell*, 1997; *Saxena*, 2017). A decision tree can be
409 applied to learn decisive attributes related to binary outcomes, for example which seismograms
410 did record dynamically triggered local seismic events, and which did not. These decisions are

made based on a set of attribute values. Consider the set of seismograms, $\boldsymbol{X}$ which are observed at a particular seismic station:

$$X = \{\overrightarrow{x_1}, \ldots \overrightarrow{x_n}\}$$

Where we can split $\boldsymbol{X}$ into $\boldsymbol{X} = \boldsymbol{X_0} \cup \boldsymbol{X_1}$, where $\boldsymbol{X_0}$ is the subset of seismograms with no signals from triggered seismicity and $\boldsymbol{X_1}$ is the subset of seismograms with signals from triggered seismicity. Each seismogram $\vec{x}$ is represented by a k-tuple of attribute values a_i

$$\vec{x} = < a_1, \ldots, a_k >$$

Then the decision-tree algorithm is designed to first select the attribute that corresponds most decisively with distinguishing the two groups of seismograms: those that recorded triggered events and those that did not. It then places this "best" attribute as well as its decisive threshold at the root of the tree (top of Figure 9a), splitting $\boldsymbol{X}$ into "left" and "right" subsets (branches) according to the attribute value. The algorithm then proceeds to calculate the next most decisive attribute for each subset. We repeat the procedure until the two groups within $\boldsymbol{X}$ are entirely separated. To begin, the entire training set is placed at the root of the tree. The order in which attributes are placed in the tree is determined by an "entropy" minimization-based statistical approach (*Mitchell*, 1997). The "entropy" represents the level of blending of members from the two sets at a particular node in the decision tree system. For each node in the tree, the quantity that is minimized with respect to the most decisive attribute's threshold value is a weighted sum of the entropies calculated for the left and right sides of the tree.

An "entropy" value E is calculated as follows:

$$E = -P_0 \log(P_0) - P_1 \log(P_1)$$

where P_l is the probability of drawing an $\vec{x} \in \boldsymbol{X_l}$ from the subset on the left or right. Clearly $E = 0$ if the subset contains elements form only one $\boldsymbol{X_l}$ and E is maximized when $\boldsymbol{X_0}$ and

$\boldsymbol{X_I}$ are equally represented. The algorithm minimizes the total entropy and so chooses the attribute and its threshold that best splits the set. In the following we apply this algorithm to seismograms from the 38 earthquakes we investigated data from, separately for each distinct region of potential triggering: tremor in Yellowstone and local earthquakes in central Utah and the Raton Basin. Because these intraplate data sets contain relatively few examples of dynamic triggering, we also apply the algorithm to a plate boundary data set of dynamic triggering collected in central California (*Chao et al.* 2012) (Figure 9). We evaluate and assign values for the following set of attributes to each seismogram: PGVZ (estimated peak stress inferred from the peak ground velocity estimated from vertical component seismograms), PGVT (estimated peak stress inferred from the peak ground velocity estimated from transverse component seismograms), TOD (local time of the day of surface wave arrival normalized to 0 being around midnight and 1 being around midday), TIDE (vertical ground velocity resulting from solid-Earth tides computed with the method of Milbert (2015), BAZ180 (back azimuth relative to 150^o, and its 180^o counterpart, $baz180 = cos^2(b\text{-}150)$, where b is the back azimuth), and BAZ90 (back azimuth relative to 150^o, and its 90^o counterparts, $baz90 = cos^2(2(b\text{-}150))$. We estimated a reference back azimuth of 150^o based on Figures 6 and 9b. As a quality-control measure, we also calculated MGVZ and MGVT, where the M stands for root-mean-square (RMS) of estimated stresses. The MGV values are reasonably well correlated with the peak stress estimates.

4.3 Decision-tree results on prevailing conditions for dynamic triggering of tremor in Yellowstone.

453 We remind the reader that station H17A recorded 28 of the 38 selected teleseismic
454 earthquakes. We detected tremor in the seismogram from earthquake #20, and potentially in
455 seismograms from earthquakes #12, #21, and #37. Although this tremor occurred during the
456 propagation of these earthquakes' surface waves, we can neither be sure that it was
457 dynamically triggered nor that it is tectonic in origin. Regardless, we applied our decision tree
458 algorithm to investigate whether conditions existed for these four earthquakes (positive
459 examples) that were different than for the other 24 (negative examples). The resulting tree is
460 shown in Figure 10.

461 The first split in the tree removes 20 of 24 negative examples from the rest because they
462 had PGVT values below 11.6 kPa, suggesting that stresses imposed by Love waves play a
463 decisive role in triggering tremor here, whichever its nature. At the next node in the tree, the
464 algorithm cleanly separates the remaining 4 negative examples from the 4 positive examples
465 by noting that surface waves for the positive examples arrive within 12^{o} from the maxima of a
466 4-lobed back-azimuthal pattern, while the negative examples are associated with more diverse
467 back azimuths that more than 12^{o} away from the lobes' maxima (Figure 6).

468

469 **4.4 Decision-tree results on prevailing conditions for dynamic triggering of local**
470 **earthquakes in central Utah**

471 Station SRU recorded 34 of the 38 teleseismic earthquakes. We detected local earthquake
472 signals in seismograms from earthquakes #21, #24, #8, #9, #10, #13, and #30. For the latter
473 five earthquake-like signals were also observed outside of the teleseismic surface wave
474 window.

475 The local earthquake potentially triggered by earthquake #8 was observed only in data
476 from station SRU. Because its signals were not observed at other stations, we did not include
477 earthquake #8's seismogram in the decision tree algorithm. We applied our decision tree
478 algorithm to investigate whether conditions existed for the remaining 6 earthquakes (positive
479 examples) that were different than for the other 27 (negative examples). The resulting tree is
480 shown in part in Figure 10 and the complete tree is shown in Figure S10.

481 The first split in the tree removes 8 negative examples from the 33 total examples based
482 on them having peak stresses *above* 6 kPa as estimated from Rayleigh waves ("vertical
483 stresses") than the 6 positive and 19 of the negative examples. Of the latter, 6 more negative
484 examples are separated out based on their surface-wave arrival azimuths being more than 21^{o}
485 away from the NW-SE axis along which the positive and remaining 13 negative examples'
486 surface waves arrive. The tree subsequently separates out another couple of small batches of
487 negative examples before it loses the ability to keep the positive examples together, further
488 splitting them in subsequent nodes. Moreover, the excluded example (#8) has a back azimuth
489 65^{o} from the reference azimuth. Including example #8 in the algorithm uses different attributes
490 at different nodes in the tree to split off small batches of negative examples, also without
491 keeping the positive ones together. This decision tree result shows that the positive examples
492 do not share attributes, such as estimates of peak stress, that distinguish them from negative
493 examples.

494 The most interesting finding is then perhaps that peak or RMS stress estimates are not
495 helpful for characterizing under which conditions local earthquakes are triggered here. This
496 implies that either prevailing conditions for dynamic earthquake triggering are independent of
497 dynamic stresses or our detections are of coincident local earthquakes rather than of

498 dynamically triggered local earthquakes. As discussed in section 3.6, the background
499 seismicity implies a 3% chance of a local earthquake occurring in a surface wave window,
500 which would provide us with about 1 detection for 33 earthquakes, yet we detected 2 clear
501 examples and 5 additional possible examples of triggering. We also deem it unlikely that our
502 detections represent quarry blasts or other anthropogenic events, given that stone-producing
503 quarries are far, and the TOD attribute did not factor into the decision tree as a prevailing
504 factor.
505
506 **4.5 Decision-tree results on prevailing conditions for dynamic triggering of local**
507 **earthquakes in the Raton Basin, Colorado**
508 Station SDCO recorded all 38 teleseismic earthquakes. We detected local earthquake
509 signals in seismograms from earthquakes #21, #23, and #24, where the latter was observed
510 only in data from station SDCO. Because this signal was not observed at other stations, we did
511 not include #24 in the decision tree algorithm. With only 2 positive examples it is not possible
512 to determine statistical significance. However, we note that the 2 positive examples both
513 occurred in 2012 and share a relatively nightly surface wave arrival time as well as a tidal
514 extremum (~ 0 vertical velocity) and have opposite back azimuths that outline the same back
515 azimuth axis as the positive examples in central Utah. The decision tree algorithm (Figure 10
516 and S11) used the latter to remove 27 of the 35 negative examples from the set based on their
517 back azimuths being more than 5^{o} away from the preferred axis. However, 8 negative examples
518 also fall along the preferred axis, and the example that was excluded (#24) is 8^{o} away from it.
519 Peak or RMS stress estimates do not enter into the decision tree, again implying that prevailing
520 conditions for dynamic earthquake triggering are independent of dynamic stresses here.

521

522 **4.6 Decision-tree results on prevailing conditions for dynamic triggering or tremor in**
523 **central California**

524 While the decision tree algorithm revealed interesting notions and successfully examined
525 prevailing conditions for the detections in the three afore-discussed intraplate regions,
526 dynamically triggered activity there is not sufficiently frequent to draw authoritative
527 conclusions. Therefore, we also applied the algorithm to a larger data set of dynamically
528 triggered tremor observed in Parkfield, central California, where the San Andreas Fault marks
529 a historic segment of the western North-American plate boundary. The observed tremor was
530 dynamically triggered by surface waves from 42 teleseismic earthquakes that occurred
531 between 2001 and 2010 (Table S1 of *Chao et al.*, 2012, see "Data and Resource" for detail
532 table link). Of these 42 earthquakes (Table S1), 12 dynamically triggered tremor in central
533 California. Previous studies (*Chao et al.*, 2012; *Peng at al.*, 2009, *Kano et al.*, 2018) suggested
534 that station PKD can be used as an indicator station for detecting triggered tremor, so we use
535 this station to calculate attributes for all 42 earthquakes. We used the same set of attributes as
536 used above, which includes dynamic stresses estimated from the vertical and transverse
537 components of seismograms recorded at station PKD as well as other potentially relevant
538 attributes: the solid-earth tide, back azimuth, and the time of day. The resulting tree is shown in
539 Figure 9.

540 The first split in the tree separates all 12 positive examples from the vast majority (26) of
541 negative ones based on the positive examples all having peak "transverse stress" (PGVT)
542 values over 1.7 kPa. Nine of the 12 positive examples also have peak "vertical stress" (PGVZ)
543 values over 3 kPa. This shows a strong correlation between peak dynamic stress estimates and

544 dynamic triggering of tremor in central California. No other attributes were needed for the
545 decision tree's determination of these prevailing conditions, with the exception of the TOD
546 attribute which separates the remaining 3 positive examples from the 4 negative examples.
547 Both these subsets have high PGVT values, on the low end of the range, and low PGVZ values,
548 on the high end of the range. This separation by TOD value shows that the 4 negative examples
549 occurred during local day time and the positive examples occurred during local night times.
550 Combined with the observation that these negative examples have stress attribute values close
551 to the thresholds, this might suggest that higher noise levels during the day (*Marcillo and*
552 *McCarthy*, 2020) may preclude the observation of modest amounts of dynamically triggered
553 tremor, that would have been detectable at night. In addition, the positive and negative
554 examples in this stress range are just within and just outside of, respectively, a 15^{o} angle from
555 the azimuthal axes of a four-lobed pattern (Figure 9), with a similar orientation as that for
556 Yellowstone. If we had not included the TOD attribute, or used the actual strike of the San
557 Andres Fault (*Eaton et al.,* 1970) as a reference back azimuth, the decision tree algorithm
558 would have used the associated BAZ90 attribute value to separate the positive and negative
559 sets in this intermediate stress range.

560 In short, the decision tree results show that transverse-component estimates of peak
561 dynamic stress is the most decisive factor as to whether seismograms in the central California
562 dataset contain triggered tremor. Prevailing conditions for dynamic triggering of tremor here
563 include peak stresses exceeding about 1.5 kPa. When peak stresses just merely exceed that
564 threshold, secondary factors like surface wave angle of incidence and time of day of the
565 detection also seem to matter. Back azimuths favorable for triggering form a 4-lobed pattern

aligned with the San Andreas Fault, which is an important observation previously recognized and explained by Hill et al. (2013).

4.7 Overall Decision-Tree Results

Our application of the decision tree algorithm to the larger tremor data set from central California (*Chao et al.*, 2012) shows that the algorithm has powerful potential for revealing the most decisive conditions for dynamically triggering tremor in a particular region. Decision tree algorithms will be particularly useful as both our attribute sets and data sets of detections of dynamically triggered seismicity continue to grow. We note that California data sets contained over a dozen (negative) examples with peak stresses less than 1 kPa, while merely a couple of intraplate examples associate with such relatively low peak stresses on account of the different data selection criteria used. Including more such "low-stress" data, from more moderate earthquakes, for the intraplate regions might paint a clearer picture of the nature of the conditions that lead to dynamic triggering there. The main results of applying the algorithm to current data from one plate-boundary and three intraplate regions are as follows.

For potentially dynamically triggered local earthquakes in both central Utah and the Raton Basin it is possible that triggering is facilitated when surface waves arrive from two favorable back azimuths, 180^{o} apart, though our detections are nowhere near numerous enough to claim statistical significance. Back azimuth might also contribute to triggering tremor in Yellowstone and central California, as a secondary factor after dynamic stresses, and include back azimuths at right angles from the NW-SE axis identified for triggering local earthquakes.

High stresses imposed by Love waves appear to be decisive for triggering *tremor* in both the Yellowstone region and Central California (Figures. 9 and 10), which is consistent with

much of the literature on dynamic triggering. However, the triggering threshold appears to be an order of magnitude higher for Yellowstone than for central California. Meanwhile, our analysis of potentially dynamically triggered local *earthquakes* in Colorado and Utah shows that these earthquakes occur independently of peak stress values estimated from surface waves.

5. Discussion

In a search for seismic events, possibly triggered by Love waves from a powerful teleseismic earthquake, in all of the conterminous United States, we confirmed the notion that seismic events are predominantly triggered in regions of high tectonic and seismic activity (the westernmost boundary of the North American tectonic plate). Within USArray data from earthquake #21 (2012 M_w 8.6 Sumatra), we did not find signals of triggered seismic events in the central and eastern USA. Consistent with these end-member findings of lots of triggered activity along the west coast and little in tectonically stable North America, we found a small number of seismic events, possibly triggered by earthquake #21 and other teleseismic earthquakes, in three locations in the western-US interior that are less seismically active than the westernmost plate boundary. Specifically, we newly detected up to four potentially triggered tremor bursts in Yellowstone, up to seven potentially triggered earthquakes in Utah, as well as three potentially triggered earthquakes in the Raton Basin, Colorado from an examination of seismograms from 38 large teleseismic earthquakes (Table 1). A decision-tree algorithm determined stress thresholds of 1.7 and 11.6 kPa for triggering tremor in central California and Yellowstone, respectively. While the California tremor is likely tectonic in nature, the Yellowstone tremor may not be. The California threshold is consistent with prior reports of stresses for which triggering has been reported (*Peng and Gomberg*, 2010; *Brodsky*

612 *and van der Elst*, 2014). Hill et al. (2013) suggest that, specifically for the San Andreas Fault
613 near Parkfield, CA, Rayleigh waves modulate tremor via pore pressure fluctuations, but that
614 the fault slip associated with the tremor is caused by SH and Love waves polarized largely
615 perpendicular or parallel to the San Andreas Fault. Figure 9 confirms this notion and shows that
616 the back azimuths for earthquakes that triggered tremor are either somewhat aligned or at right
617 angles with the San Andreas Fault's strike.

618 Dynamically triggered events are hard to detect in raw seismograms, their identification
619 can be negatively affected by various types of noise, including anthropogenic seismic noise
620 (*Diaz et al.,* 2017; *Marcillo and McCarthy, 2020*) and instrumental quirks or adjustments, such
621 as mass centerings or calibrations, or might coincide with, large earthquakes' surface waves,
622 rather than be triggered by them. For example, upon first examination, we observed two
623 candidate triggered earthquakes in Minnesota after earthquake #21. A subsequent closer
624 inspection did not reject the candidate triggered events since the signals shared characteristics
625 with triggered earthquake signals. However, after inspection of hours and days of seismograms
626 before and after the earthquake, we rejected both candidates because a multitude of similar
627 signals, possibly from anthropogenic events, implied a high likelihood for one of these events
628 coinciding with the earthquake's surface waves by chance. Through the use of visual
629 inspection in addition to timing- and frequency-based selection criteria for these seismic
630 phenomena, our search yielded numerous false positives, illustrating the challenge posed by
631 moving from *ad-hoc* observations of dynamic triggering to a systematic search that also
632 includes a catalog of teleseismic events that did not dynamically trigger other events, even
633 when large stress variations were supplied.

Table 1 presents the 38 teleseismic earthquakes used in our study, up to 11 of which produced potentially triggered events in three western intraplate regions. Our observations, analyses, and decision-tree results confirm the greater likelihood for triggered *tremor* from high dynamic stress surface waves, as reported in the literature. Our results also indicate that triggered *earthquakes* are *not* positively correlated with high dynamic stress surface waves, in agreement with (*Wang et al*., 2018). On the contrary, our analysis shows that back-azimuth appears to be an important factor, for both earthquakes and tremor, in whether dynamic triggering occurs or not. A large number of surface waves (Table S2) with favorable back-azimuths (Figure 6), are not associated with triggering, which argues for future multi-attribute analyses, including stress values estimated at depth within the crust, all components of the dynamic stress tensors from largely coeval Love and Rayleigh waves, and how dynamic stress tensors translate to stress quantities other than peak stress estimates that matter to faulting.

The application of a decision-tree machine-learning algorithm to an existing and a new data set of likely triggered events has provided us with several insights:

1. Prevailing conditions for triggering tremor in central California and Yellowstone decisively include peak stresses estimated from Love waves,
2. The stress threshold for triggering tremor in central California is just under 2 kPa,
3. The stress threshold for triggering tremor in Yellowstone is just over 10 kPa,
4. The arrival azimuth of surface waves appears to be important in whether surface waves can trigger local tremor or earthquakes,
5. Peak dynamic stress values do not appear to be important for triggering local

earthquakes, at least in Utah and Colorado,

6. To unleash the full power of decision tree algorithms, more data are needed that provide examples of both the occurrence *and* absence of dynamic triggering under different conditions at plate boundaries and in intraplate regions.

6. Conclusions

Reports about dynamically triggered seismic events are regularly published in the professional literature (*Freed*, 2005; *Gonzalez-Huizar et al.*, 2012; *Aiken and Peng*, 2014; *Yao et al.*, 2015; *Johnson et al.*, 2015; *Bansal et al.*, 2016; *Bansal et al.*, 2018; *Opris et al.*, 2018; *Prejean and Hill*, 2018; *Wang et al.*, 2018), yet many aspects about the physical mechanisms leading to such triggering remain elusive. Documenting instances of dynamically triggered seismic events and the conditions under which they occur and not occur provide us with data to illuminate some of these aspects. In this paper we approached this challenge from multiple different perspectives:

1. We used a decision tree algorithm and rose diagrams (Figures 6, 9, and 10) to determine that the back-azimuth of surface waves could be an important factor in dynamic triggering.
2. The algorithm further showed that dynamic stresses from Love waves are, as expected by practitioners, the most important attribute for triggering tectonic tremor in central California and Yellowstone.
3. We examined each seismogram recorded anywhere in the conterminous US of the 11 April 2012 M_w 8.6 Sumatra earthquake as to whether a dynamically triggered seismic event was recorded. We did not find any such events in the central and eastern USA. However, we

found several dozens of records of dynamically triggered events along the western edge of the North American Plate, which align with previous reports in the literature.

4. Dynamically triggered tremor was newly detected in the Yellowstone hotspot region, which could be hydrothermal in origin, and dynamically triggered earthquakes were newly detected in central Utah and southeastern Colorado, near the Raton Basin.
5. Our experiments with automating such detections have so far been thwarted by instrumental quirks and adjustments, anthropogenic noise, and/or signal-generated noise. We detected a sizable number of "false triggers" during the examinations discussed in this paper. A "false trigger" is a seismic record that looks like a record of tremor or an earthquake but is rather a record of one of the above-listed noise signals.
6. We examined seismograms from 37 additional worldwide earthquakes that were recorded near Yellowstone, central Utah, and the Raton Basin. This examination identified additional possibly dynamically triggered seismic events in these three regions.
7. Application of the aforementioned decision tree further revealed that peak dynamic stresses estimated from teleseismic surface waves does not appear to correlate with whether or not a local earthquake is triggered.

Acknowledgements and Data

This research is funded by the Integrated Data-Driven Discovery in Geophysical and Astrophysical Sciences (IDEAS) program under National Science Foundation grant NSF-NRT 1450006, and by Northwestern University's Data Science Initiative (DSI). We are grateful to Boris Rösler for stimulating discussions. We thank Hector Gonzalez-Huizar and two

anonymous reviewers for critical reviews that helped us to significantly improve the manuscript.

All seismic data were downloaded through the IRIS Wilber 3 system (http://ds.iris.edu/wilber3/find_event) or IRIS Web Services, including the following seismic networks (http://ds.iris.edu/mda): (1) the AZ (ANZA; UC San Diego, 1982); (2) the TA (Transportable Array; IRIS, 2003); (3) the US (USNSN, Albuquerque, 1990); (4) the IU (GSN; Albuquerque, 1988); (5) the BK (BDSN; NCEDC, 2014); (6) the CI (SCSN; California, 1926); (7) the XI (SPREE; Van der Lee et al., 2011); (8) the II (GSN; SIO, 1986); (9) the NN (Nevada, 1971); (10) the UO (U. of Oregon; UOPNSN, 1990); (11) the UW (PNSN, 1963); (12) the YW (FACES; Brudzinski and Allen, 2007); (13) the Z9 (SESAME; Fischer et al., 2010); (14) the YX (NE-NV BB; Klemperer and Miller, 2010); (15) the XQ (FAME; Levander, 2007); (16) the 7A (MAGIC; Long and Wiita, 2013); (17) the XU (CAFE; Malone et al., 2006); (18) the XR (SIEDCAR; Pulliam et al., 2008); (19) the XO (OIINK; Pavlis and Gilbert, 2011); (20) the XT (IDOR; Russo ,2011); (21) the UU (UURSN; Utah, 1962).

The ANSS (Advanced National Seismic System) earthquake catalog can be accessed at https://earthquake.usgs.gov/data/comcat/. Solid tide data can be accessed at http://geodesyworld.github.io/SOFTS/solid.htm.

References

Professional papers

Aiken, C., and Z. Peng (2014), Dynamic triggering of microearthquakes in three geothermal/volcanic regions of California, *J. Geophys. Res. Earth*, *119*, 6992–7009, doi:10.1002/ 2014JB011218.

724 Bockholt, B. M., Langston, C. A., DeShon, H. R., Horton, S., & Withers, M. (2014),
725 Mysterious tremor-like signals seen on the Reelfoot Fault, northern Tennessee, *Bulletin of*
726 *the Seismological Society of America*, *104*(5), 2194-2205, doi:10.1785/0120140030**.**
727 Bansal, A. R., D. Yao, Z. Peng, and D. Sianipar (2016), Isolated regions of remote triggering in
728 South/Southeast Asia following the 2012 Mw8.6 Indian Ocean earthquake, *Geophys. Res.*
729 *Lett.*, *43*(20), 10,654-10,662, doi:10.1002/2016GL069955.
730 Bansal, A. R., N. P. Rao, Z. Peng, D. Shashidhar, and X. Meng (2018), Remote Triggering in
731 the Koyna-Warna Reservoir-Induced Seismic Zone, Western India, *J. Geophys. Res.*
732 *Solid Earth*, *123*(3), 2318–2331, doi:10.1002/2017JB014563.
733 Brodsky, E. E., and N. J. van der Elst (2014), The Uses of Dynamic Earthquake Triggering,
734 *Annu. Rev. Earth Planet. Sci.*, *42*(1), 317–339,
735 doi:10.1146/annurev-earth-060313-054648.
736 Chao, K., Peng, Z., Gonzalez□Huizar, H., Aiken, C., Enescu, B., Kao, H., Vaelasco A.A.,
737 Obara, K. and T. Matsuzawa (2013). A global search for triggered tremor following the
738 2011 M w 9.0 Tohoku earthquake. *Bulletin of the Seismological Society of*
739 *America*, *103*(2B), 1551-1571.
740 Chao, K., and K. Obara (2016), Triggered tectonic tremor in various types of fault systems of
741 Japan following the 2012 M_w 8.6 Sumatra earthquake, *J. Geophys. Res. Solid Earth*,
742 *121*(1), 170–187, doi:10.1002/2015JB012566.
743 Chao, K., and C. Yu (2018), A MATLAB GUI for Examining Triggered Tremor: A Case Study
744 in New Zealand, *Seismol. Res. Lett.*, doi:10.1785/0220180057.
745 Chao, K., Z. Peng, A. Fabian, and L. Ojha (2012), Comparisons of triggered tremor in
746 California, *Bull. Seismol. Soc. Am.*, *102*(2), 900–908, doi:10.1785/0120110151.

747 Chao, K., Z. Peng, Y.-J. Hsu, K. Obara, C. Wu, K.-E. Ching, S. van der Lee, H.-C. Pu, P.-L.
748 Leu, and A. Wech (2017), Temporal variation of tectonic tremor activity in southern
749 Taiwan around the 2010 ML6.4 Jiashian earthquake, *J. Geophys. Res. Solid Earth*, *122*(7),
750 5417–5434, doi:10.1002/2016JB013925.
751 Chao, K., Z. Peng, W. B. Frank, G. A. Prieto, and K. Obara (2019), Isolated Triggered Tremor
752 Spots in South America and Implications for Global Tremor Activity, *Seismol. Res. Lett.*,
753 *90*(5), 1726–1739, doi:10.1785/0220190009.
754 Castro, R. R., González□Huízar, H., Ramón Zúñiga, F., Wong, V. M., & Velasco, A. A.
755 (2015). Delayed dynamic triggered seismicity in northern Baja California, México caused
756 by large and remote earthquakes. *Bulletin of the Seismological Society of America*, *105*(4),
757 1825-1835, doi:10.1785/0120140310.
758 Castro, R. R., Clayton, R., Hauksson, E., & Stock, J. (2017). Observations of remotely
759 triggered seismicity in Salton Sea and Coso geothermal regions, Southern California,
760 USA, after big (MW> 7.8) teleseismic earthquakes. *Geofísica internacional*, *56*(3),
761 269-286.
762 Canitano, A., Gonzalez-Huizar, H., Hsu, Y. J., Lee, H. M., Linde, A. T., & Sacks, S. (2019).
763 Testing the influence of static and dynamic stress perturbations on the occurrence of a
764 shallow, slow slip event in eastern Taiwan. *Journal of Geophysical Research: Solid*
765 *Earth*, *124*(3), 3073-3087.
766 Cerda, I., H. Gonzalez-Huizar, A. A. Velasco, D. L. Kilb, and K. L. Pankow (2011),
767 Systematic Analysis of Dynamic Earthquake Triggering Using the EarthScope'ss
768 USArray Data, Eos Trans. AGU, Fall Meet. Suppl., abstract S13A-2258.

769 Delaney, P. T., and A. E. Gartner (1997), Physical processes of shallow mafic dike
770 emplacement near the San Rafael Swell, Utah, *Geol. Soc. Am. Bull.*, *109*(9), 1177–1192,
771 doi:10.1130/0016-7606(1997)109<1177:PPOSMD>2.3.CO;2.
772 Díaz, J., Ruiz, M., Sánchez-Pastor, P. S., & Romero, P. (2017), Urban seismology: On the
773 origin of earth vibrations within a city. *Scientific reports*, *7*(1), 1-11.
774 Eaton, J. P., M. E. O'Neill, and J. N. Murdock (1970), Aftershocks of the 1966 Parkfield–
775 Cholame, California earthquake: a detailed study, *Bull. Seism. Soc. Am.* **60,** 1151–1197.
776 Freed, A. M. (2005), Earthquake Triggering by Static, Dynamic, and Postseismic Stress
777 Transfer, *Annu. Rev. Earth Planet. Sci.*, *33*(1), 335–367,
778 doi:10.1146/annurev.earth.33.092203.122505.
779 Goldstein, P. A. U. L., and A. Snoke (2005), SAC availability for the IRIS
780 community. *Incorporated Research Institutions for Seismology Newsletter*, *7*
781 (UCRL-JRNL-211140).
782 Gomberg, J., J. L. Rubinstein, and Z. Peng (2008), Widespread triggering of nonvolcanic
783 tremor in California, *Science (80-.).*, *319*, 173, doi:10.1126/science.1149164.
784 Gomberg, J., and S. Prejean (2013), Triggered tremor sweet spots in Alaska, *J. Geophys. Res.*
785 *Earth*, *118*(12), 6203–6218, doi:10.1002/2013JB010273.
786 Gonzalez-Huizar, H., A. A. Velasco, Z. Peng, and R. Castro (2012), Remote triggered
787 seismicity caused by the 2011, M9.0 Tohoku, Japan earthquake, *Geophys. Res. Lett*,
788 *L10302*, doi:10.1029/2012GL051015.
789 Hill, D. P., Z. Peng, D. R. Shelly, and C. Aiken (2013), S-Wave Triggering of Tremor beneath
790 the Parkfield, California, Section of the San Andreas Fault by the 2011 Tohoku, Japan,

Earthquake: Observations and Theory, *Bull. Seismol. Soc. Am.*, *103*(2B), 1541–1550, doi:10.1785/0120120114.

Hill, D. P., and S. G. Prejean (2015), Dynamic Triggering, in *Treatise on Geophysics*, vol. 4, pp. 273–304, Elsevier.

Hurwitz, Shaul, Robert A. Sohn, Karen Luttrell, and Michael Manga. "Triggering and modulation of geyser eruptions in Yellowstone National Park by earthquakes, earth tides, and weather." *Journal of Geophysical Research: Solid Earth* 119, no. 3 (2014): 1718-1737.

Huang, H. H., F. C. Lin, B. Schmandt, J. Farrell, R. B. Smith, and V. C. Tsai (2015), The Yellowstone magmatic system from the mantle plume to the upper crust, *Science (80-.).*, *348*(6236), 773–776, doi:10.1126/science.aaa5648.

Husen, S., S. Wiemer, and R. B. Smith (2004), Remotely Triggered Seismicity in the Yellowstone National Park Region by the 2002 Mw 7.9 Denali Fault Earthquake, Alaska, *Bull. Seismol. Soc. Am.*, *94*(6B), S317–S331, doi:10.1785/0120040617.

Johnson, C. W., R. Bürgmann, and F. F. Pollitz (2015), Rare dynamic triggering of remote *M* $\geq$5.5 earthquakes from global catalog analysis, *J. Geophys. Res. Solid Earth*, *120*(3), 1748–1761, doi:10.1002/2014JB011788.

Kato, A., Fukuda, J. I., & Obara, K. (2013), Response of seismicity to static and dynamic stress changes induced by the 2011 M9. 0 Tohoku-Oki earthquake, *Geophysical research letters*, *40*(14), 3572-3578, doi:10.1002/grl.50699.

Kundu, B., Ghosh, A., Mendoza, M., Bürgmann, R., Gahalaut, V. K., & Saikia, D. (2016), Tectonic tremor on Vancouver Island, Cascadia, modulated by the body and surface

waves of the Mw 8.6 and 8.2, 2012 East Indian Ocean earthquakes. *Geophysical Research Letters*, *43*(17), 9009-9017, doi: 10.1002/2016GL069755.

Kano, M. et al. (2018), Development of a Slow Earthquake Database, *Seismol. Res. Lett.*, *89*(4), 1566–1575, doi:10.1785/0220180021.

Linville, L., Pankow, K., Kilb, D., & Velasco, A. (2014), Exploring remote earthquake triggering potential across EarthScopes' Transportable Array through frequency domain array visualization. *Journal of Geophysical Research: Solid Earth*, *119*(12), 8950-8963, doi:10.1002/2014JB011529.

Lecun, Y., Y. Bengio, and G. Hinton (2015), Deep learning, *Nature*, *521*(7553), 436–444, doi:10.1038/nature14539.

Marcillo, O. E., & MacCarthy, J. (2020). Mapping Seismic Tonal Noise in the Contiguous United States. *Seismological Research Letters*, *91*(3), 1707-1716, doi: 10.1785/0220190355.

Meng, L., Ampuero, J. P., Stock, J., Duputel, Z., Luo, Y., & Tsai, V. C. (2012), Earthquake in a maze: Compressional rupture branching during the 2012 Mw 8.6 Sumatra earthquake. *Science*, *337*(6095), 724-726, doi: 10.1126/science.1224030.

Milbert, D. (2015), Solid earth tide program: solid. Retrieved August 10, 2018, *from http//geodesyworld, github, io/SOFTS/solid.htm*, written in fortran.

Mitchell, T. M. (Tom M. (1997), *Machine Learning*, 1st ed., McGraw-Hill.

Nakai, J. S., M. Weingarten, A. F. Sheehan, S. L. Bilek, and S. Ge (2017), A Possible Causative Mechanism of Raton Basin, New Mexico and Colorado Earthquakes Using Recent Seismicity Patterns and Pore Pressure Modeling, *J. Geophys. Res. Solid Earth*, *122*(10), 8051–8065, doi:10.1002/2017JB014415.

836 Opris, A., B. Enescu, Y. Yagi, and J. Zhuang (2018), Triggering and decay characteristics of
837 dynamically activated seismicity in Southwest Japan, *Geophys. J. Int.*, *212*(2), 1010–1021,
838 doi:10.1093/gji/ggx456.
839 Pankow, K. L., W. J. Arabasz, J. C. Pechmann, and S. J. Nava (2004), Triggered Seismicity in
840 Utah from the 3 November 2002 Denali Fault Earthquake, *Bull. Seismol. Soc. Am.*,
841 *94*(6B), S332–S347, doi:10.1785/0120040609.
842 Peng, Z., J. E. Vidale, A. G. Wech, R. M. Nadeau, and K. C. Creager (2009), Remote triggering
843 of tremor along the San Andreas Fault in central California, *J. Geophys. Res.*,
844 *114*(B00A06), doi:10.1029/2008JB006049.
845 Peng, Z., and J. Gomberg (2010), An integrated perspective of the continuum between
846 earthquakes and slow-slip phenomena, *Nat. Geosci.*, *3*, 599–607, doi:10.1038/ngeo940.
847 Prejean, S. G., D. P. Hill, E. E. Brodsky, S. E. Hough, M. J. S. Johnston, S. D. Malone, D. H.
848 Oppenheimer, A. M. Pitt, and K. B. Richards-Dinger (2004), Remotely triggered
849 seismicity on the United States west coast following the Mw 7.9 Denali fault earthquake,
850 *Bull. Seismol. Soc. Am.*, *94*(6B), S348–S359.
851 Prejean, S. G., and D. P. Hill (2018), The influence of tectonic environment on dynamic
852 earthquake triggering: A review and case study on Alaskan volcanoes, *Tectonophysics*,
853 *745*, 293–304, doi:10.1016/J.TECTO.2018.08.007.
854 Ramirez, J., and F. G. Meyer (2011), Machine learning for seismic signal processing: Seismic
855 phase classification on a manifold, in *Proceedings - 10th International Conference on*
856 *Machine Learning and Applications, ICMLA 2011*, vol. 1, pp. 382–388.
857 Rubinstein, J. L., J. Gomberg, J. E. Vidale, A. G. Wech, H. Kao, K. C. Creager, and G. Rogers
858 (2009), Seismic wave triggering of nonvolcanic tremor, episodic tremor and slip, and

earthquakes on Vancouver Island, *J. Geophys. Res.*, *114*(B00A01), doi:10.1029/2008JB005875.

Rösler, B., & van der Lee, S. (2020), Using Seismic Source Parameters to Model Frequency-Dependent Surface-Wave Radiation Patterns, Seismol. Res. Lett. 91, 992–1002, doi: 10.1785/0220190128.

Saxena, R. (2017), Building Decision Tree Algorithm, *Retrieved May 23, 2018, from https//dataaspirant.com/2017/02/01/decision-treealgorithm-python-with-scikit-learn/.*

Tang, V., Seetharaman, P., Chao, K., Pardo, A. B. and S. van der Lee (2020), Automating the Detection of Dynamically Triggered Earthquakes via a Deep Metric Learning Algorithm. Seismological Redearch Letters, doi:10.1785/0220190165.

Velasco, A., S. Hernandez, and T. Parsons (2008), Global Ubiquity of Dynamic Earthquake Triggering, *Nat. Geosci*, *1*, 375–379, doi:10.1038/ngeo204.

Vandemeulebrouck, J., Roux, P., & Cros, E. (2013), The plumbing of Old Faithful Geyser revealed by hydrothermal tremor. *Geophysical Research Letters*, *40*(10), 1989-1993, doi: 10.1002/grl.50422.

Van der Elst, N. J., H. M. Savage, K. M. Keranen, and G. A. Abers (2013), Enhanced Remote Earthquake Triggering at Fluid-Injection Sites in the Midwestern United States, *Science (80-.).*, *341*(September), 1380–1385, doi:10.1126/science.1238948.

Velasco, A., R. Alfaro-Diaz, and D. Kilb (2016), A Time-Domain Detection Approach to Identify Small Earthquakes within the Continental United States Recorded by the USArray and Regional Networks, *Bull.*

Wang, B., Harrington, R. M., Liu, Y., Kao, H., & H. Yu (2019), Remote Dynamic Triggering of Earthquakes in Three Unconventional Canadian Hydrocarbon Regions Based on a

Multiple-Station Matched-Filter Approach. *Bulletin of the Seismological Society of America*, *109*(1), 372-386.

Yao, D., Z. Peng, and X. Meng (2015), Remotely triggered earthquakes in South-Central Tibet following the 2004 Mw 9.1 Sumatra and 2005 Mw 8.6 Nias earthquakes, *Geophys. J. Int.*, *201*(2), 543–551, doi:10.1093/gji/ggv037.

Yeck, W. L., Weingarten, M., Benz, H. M., McNamara, D. E., Bergman, E. A., Herrmann, R. B., ... & Earle, P. S. (2016), Far-field pressurization likely caused one of the largest injection induced earthquakes by reactivating a large preexisting basement fault structure. *Geophysical Research Letters*, *43*(19), 10-198.

Data Sources

Albuquerque Seismological Laboratory (ASL)/USGS (1988), Global Seismograph Network - IRIS/USGS. International Federation of Digital Seismograph Networks. Dataset/Seismic Network, doi:10.7914/SN/IU.

Albuquerque Seismological Laboratory (ASL)/USGS (1990), United States National Seismic Network. International Federation of Digital Seismograph Networks. Dataset/Seismic Network, doi:10.7914/SN/US.

Brudzinski, M. and R. Allen (2007), Resolving structural control of episodic tremor and slip along the length of Cascadia. International Federation of Digital Seismograph Networks. Dataset/Seismic Network, doi:10.7914/SN/YW_2007.

California Institute of Technology and United States Geological Survey Pasadena (1926), Southern California Seismic Network. International Federation of Digital Seismograph Networks. Dataset/Seismic Network, doi:10.7914/SN/CI.

905 Fischer, K. M., Hawman, R. B. and L. S. Wagner (2010), Southeastern Suture of the
906 Appalachian Margin Experiment. International Federation of Digital Seismograph
907 Networks. Dataset/Seismic Network, doi:10.7914/SN/Z9_2010.
908 IRIS Transportable Array (2003), USArray Transportable Array. International Federation of
909 Digital Seismograph Networks. Dataset/Seismic Network, doi:10.7914/SN/TA.
910 Klemperer, S. and K. Miller (2010), Flexarray 3D Passive Seismic Imaging of Core-Complex
911 Extension in the Ruby Range Nevada. International Federation of Digital Seismograph
912 Networks. Dataset/Seismic Network, doi:10.7914/SN/YX_2010.
913 Levander, A. (2007), Seismic and Geodetic Investigations of Mendocino Triple Junction
914 Dynamics. International Federation of Digital Seismograph Networks. Dataset/Seismic
915 Network, doi:10.7914/SN/XQ_2007.
916 Long, M. and P. Wiita (2013), Mid-Atlantic Geophysical Integrat ive Collaboration.
917 International Federation of Digital Seismograph Networks. Dataset/Seismic Network,
918 doi:10.7914/SN/7A_2013.
919 Northern California Earthquake Data Center (2014). *Berkeley Digital Seismic Network*
920 *(BDSN)*. Northern California Earthquake Data Center, doi:10.7932/BDSN.
921 Malone, S., Creager, K., Rondenay, S., Melbourne, T. and G. Abers (2006), Collaborative
922 Research: Earthscope integrated investigations of Cascadia subduction zone tremor,
923 structure and process. International Federation of Digital Seismograph Networks.
924 Dataset/Seismic Network, doi:10.7914/SN/XU_2006.
925 Pulliam, J., Grand, S. and J. Sansom (2008), Seismic Investigation of Edge Driven Convection
926 Associated with the Rio Grande Rift. International Federation of Digital Seismograph
927 Networks. Dataset/Seismic Network, doi:10.7914/SN/XR_2008.

928 Pavlis, G. and H. Gilbert (2011), Ozark Illinois Indiana Kentucky (OIINK) Flexible Array
929 Experiment. International Federation of Digital Seismograph Networks. Dataset/Seismic
930 Network, doi:10.7914/SN/XO_2011.
931 Russo, R. (2011), Deformation and Magmatic Modification of a Steep Continental Margin,
932 Western ID-Eastern OR. International Federation of Digital Seismograph Networks.
933 Dataset/Seismic Network, doi:10.7914/SN/XT_2011.
934 Scripps Institution of Oceanography (1986): Global Seismograph Network - IRIS/IDA.
935 International Federation of Digital Seismograph Networks. Dataset/Seismic Network, doi:
936 10.7914/SN/II.
937 University of Utah (1962): University of Utah Regional Seismic Network. International
938 Federation of Digital Seismograph Networks. Dataset/Seismic Network, doi:
939 10.7914/SN/UU.
940 University of Washington (1963): Pacific Northwest Seismic Network. International
941 Federation of Digital Seismograph Networks. Dataset/Seismic Network,
942 doi:10.7914/SN/UW.
943 University of Nevada, Reno (1971), Nevada Seismic Network. International Federation of
944 Digital Seismograph Networks. Dataset/Seismic Network, doi:10.7914/SN/NN.
945 UC San Diego (1982), ANZA Regional Network. International Federation of Digital
946 Seismograph Networks. Dataset/Seismic Network. 10.7914/SN/AZ.
947 University of Oregon (1990), University of Oregon and Pacific Northwest Seismic Network.
948 International Federation of Digital Seismograph Networks. Dataset/Seismic Network,
949 doi:10.7914/SN/UO.

Van der Lee, S., Wiens, D., Revenaugh, J., Frederiksen, A. and F. Darbyshire (2011), Superior Province Rifting Earthscope Experiment. International Federation of Digital Seismograph Networks. Dataset/Seismic Network, doi:10.7914/SN/XI_2011.

Figure Captions

Figure 1. Examples of dynamic triggering of triggered tremor (a) and triggered earthquakes (b) during the surface wave trains of earthquakes #20 (20 March 2012 M_w 7.5 Mexico) and #24 (05 September 2012 M_w 7.6 Costa Rica), respectively. From bottom to top: Raw, vertical-component seismogram; Same as in bottom frame but zoomed in to the pink-highlighted time window; Spectrogram of the band-passed zoomed-in, vertical-component seismogram, the band's corner frequencies are 2 and 8 Hz; the top three frames are band-passed vertical-, north-, and east-component seismograms of the zoomed-in time window. Y-axis units are in m/s for band-passed waveforms and counts for raw data.

Figure 2. Zoomed-out (a) and zoomed-in (b) snapshots of CrazyTremor, a MATLAB GUI-based software package for finding and locating triggered events (Chao and Yu, 2018). Seismograms shown from 8 nearby stations in Utah include seismic waves from the 11 April 2012 M_w 8.6 Sumatra earthquake and a local, potentially triggered earthquake. Seismograms are from the University of Utah Regional Seismic Network, which was virtually part of USArray. Frames, clockwise from top left: CrazyTremor menu determining which type of seismogram data are shown in the top center frame; seismograms from multiple seismic stations during the same time window (station names are indicated to the top right of this frame; the user can pick P and S arrival times in this window with their mouse); map of stations

(triangles) and local-earthquake epicenter (black star); Map parameter menu; Figure and data loading menu; Raw data from one station (SRU); Menu for determining which type of seismogram data are shown in bottom center frame. Local triggered earthquakes appear on the 2–8 Hz band-pass filtered seismograms at ~5420 seconds. The bottom panel shows a seismogram of station SRU (red triangle).

Figure 3. Top: Map of USArray and affiliated stations (triangles) that recorded earthquake #21 (11 April 2012 M_w8.6 Sumatra). Green-colored stations recorded signals from triggered events, all other-colored stations did not. Bottom: Seismogram panels with the same layout as in Figure 1, showing data from each of the three intraplate regions where we report potentially triggered local events: tremor in Yellowstone (left), and earthquakes in Utah (center) and the Raton Basin, Colorado (right).

Figure 4. Map of epicenters of 38 large triggering earthquakes (green stars) and stations (triangles) whose data we examined for triggered events. Blue stations recorded at least one potentially triggered earthquake. The red station (H17A) recorded at least one potentially triggered tremor. Nearby yellow stations did not show signals from triggered events above the noise level. Epicenters with red outlines are associated with potential triggering in at least one of three intraplate locations: Yellowstone, Utah, and the Raton Basin, Colorado.

Figure 5. Map of earthquake (grey circles) from 2004 to 2017 in Yellowstone, Utah, and Colorado from the USGS (https://earthquake.usgs.gov/). The size of the grey circles depends on the magnitude of the earthquake. Red triangles are stations for which we detected at least

one potentially triggered local event. Green stars represent epicenters of the local earthquake potentially triggered by surface waves from the teleseismic earthquakes in Table 3 and 4.

Figure 6. Distribution of studied events, as a function of back azimuth. Top: Yellowstone, represented by station H17A; Middle: central Utah, represented by station SRU; Bottom: Raton Basin, Colorado, represented by station SDCO. Each bar represents a large global earthquake, with bar length proportional to the estimated peak dynamic stress (in kPa) inferred from Rayleigh waves (left) and Love waves (right), and bar color representing whether a local event was likely triggered (blue & green), maybe triggered (cyan), or not triggered (red & orange).

Figure 7. Seismograms of earthquake #21 (11 April 2012 Mw8.6 Sumatra). The layout is the same as in Figure 1, except the top three frames are replaced by a multi-frame panel that represents band-passed vertical component seismograms from a group of nearby stations that all recorded a potentially triggered earthquake in central Utah.

Figure 8. Seismograms of possible triggered earthquakes in Colorado following the 11 April 2012 M_w 8.6 Sumatra earthquake. Blue seismograms and the spectrogram show the repetitive station SDCO and black seismograms are represented records from nearby stations. Seismograms of earthquake #21 (11 April 2012 M_w 8.6 Sumatra). The layout is the same as in Figure 7. The seismograms shown are from a group of stations that all recorded a potentially triggered earthquake in the Raton Basin, Colorado.

Figure 9. Results from the decision-tree algorithm described in the text applied to a known distribution of global earthquakes whose surface waves either did or did not trigger local tremor in central California (*Chao et al*., 2012) (a) and the distribution of these earthquakes as a function of azimuth (b). Bar length and color as in Figure 6. Decision-tree attribute names "PGVZ", "PGVT", and "TOD" are defined in the text. The branches' "entropy" is labeled "E", a value of 0 means that all members of that branch belong to the same class and a value near 1 means that the members of that branch are about evenly split between two classes: triggered (green numbers) and not triggered (red numbers).

Figure 10. Decision-tree results for the three intraplate regions: Yellowstone, represented by station H17A (a), central Utah, represented by station SRU (b) and the Raton Basin, Colorado, represented by station SDCO (c). Complete trees for the latter two, including less-decisive branches, are provided in Figures S10 and S11. "Entropy", colored numbers, and attribute names are as in Figure 9. Additional decision-tree attribute names "BAZ90", "BAZ180", and "TIDE" are defined in the text.

Figure 1.

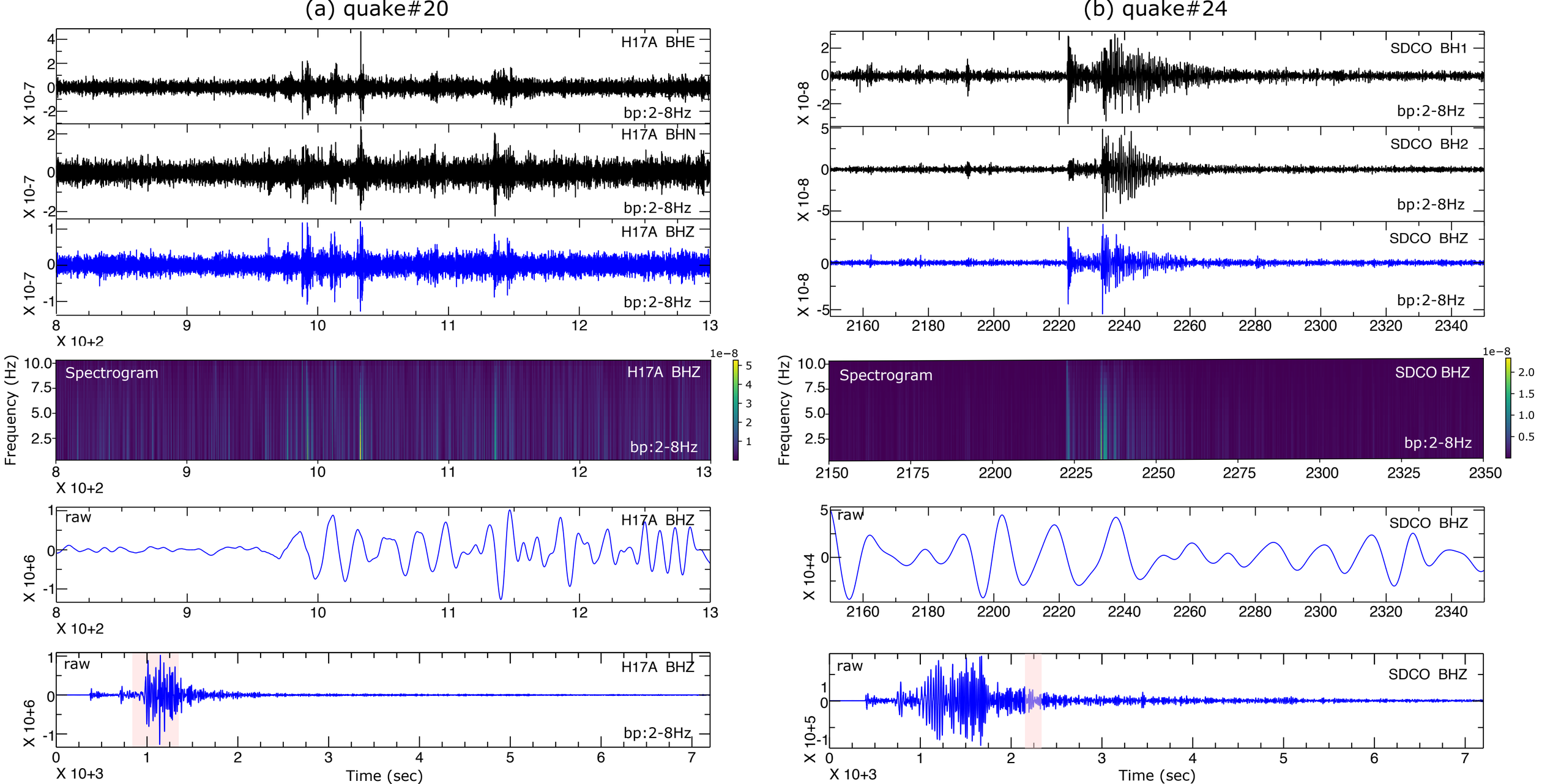
(a) quake#20
(b) quake#24
H17A BHE
H17A BHN
H17A BHZ
SDCO BH1
SDCO BH2
SDCO BHZ
bp:2-8Hz
X 10-7
X 10-8
X 10+2
Spectrogram
Frequency (Hz)
1e−8
raw
X 10+6
X 10+4
X 10+5
X 10+3
Time (sec)

Figure 2.

(a) Tirggered earthquake in Utah following the 2012/04/11 Mw8.6 event

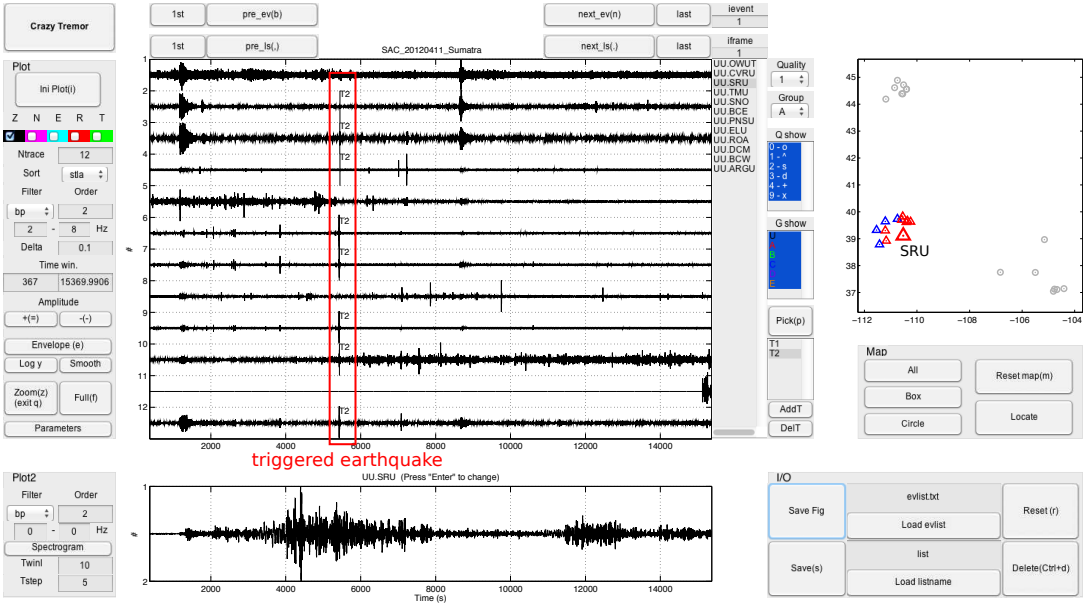

(b) Zoom-in seismograms of the triggered earthquake

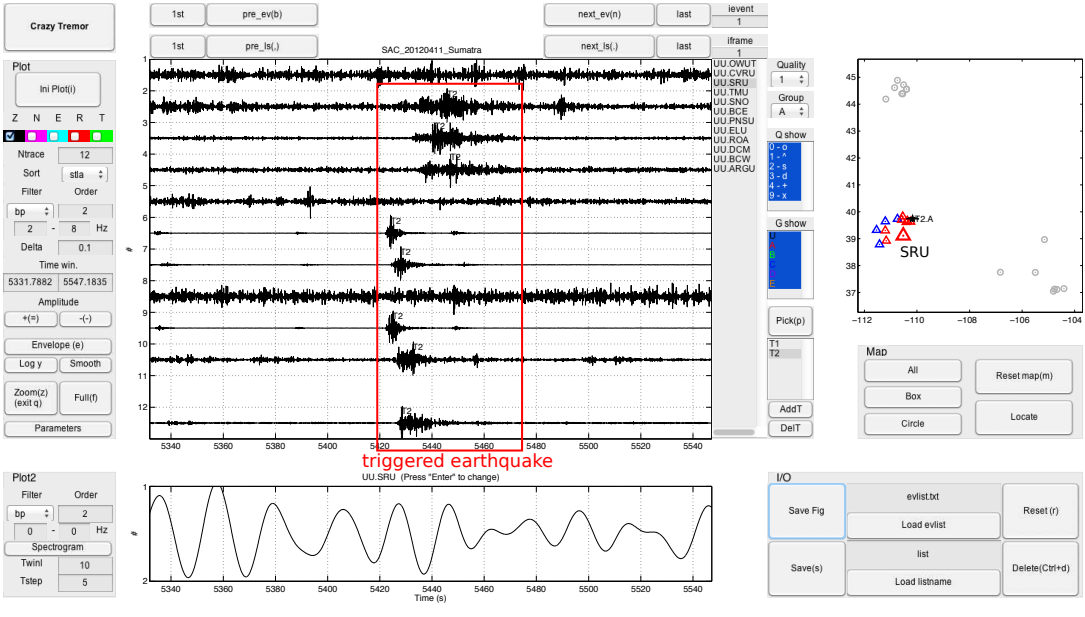

Figure 3.

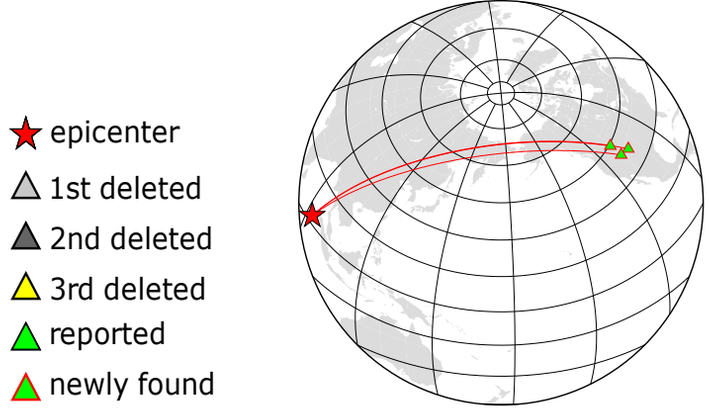

11 April 2012 M_w8.6 Sumatra

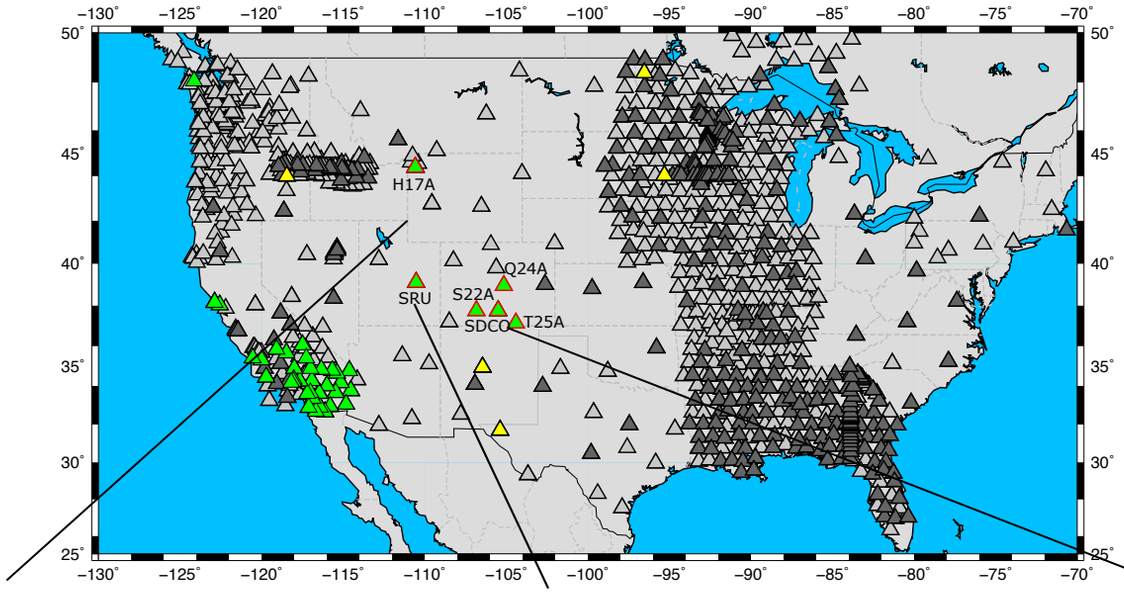

Yellowstone (station H17A)

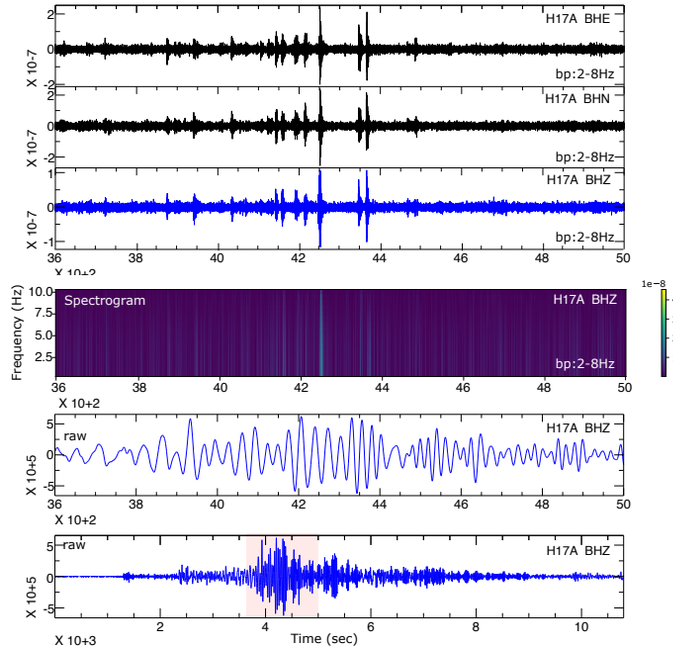

Utah (station SRU)

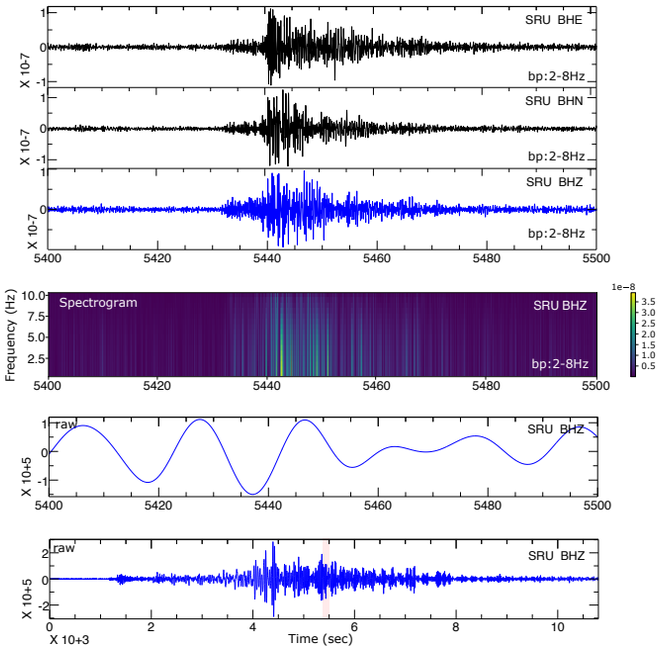

Colorado (station SDCO)

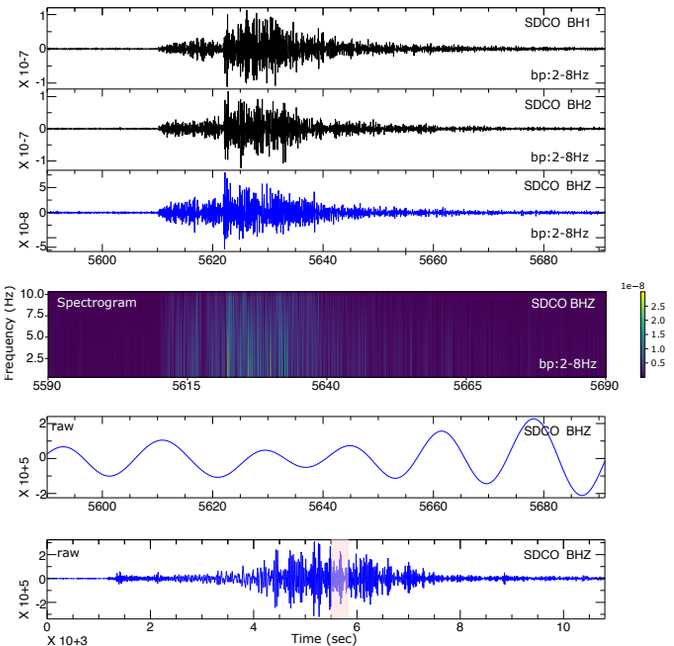

Figure 4.

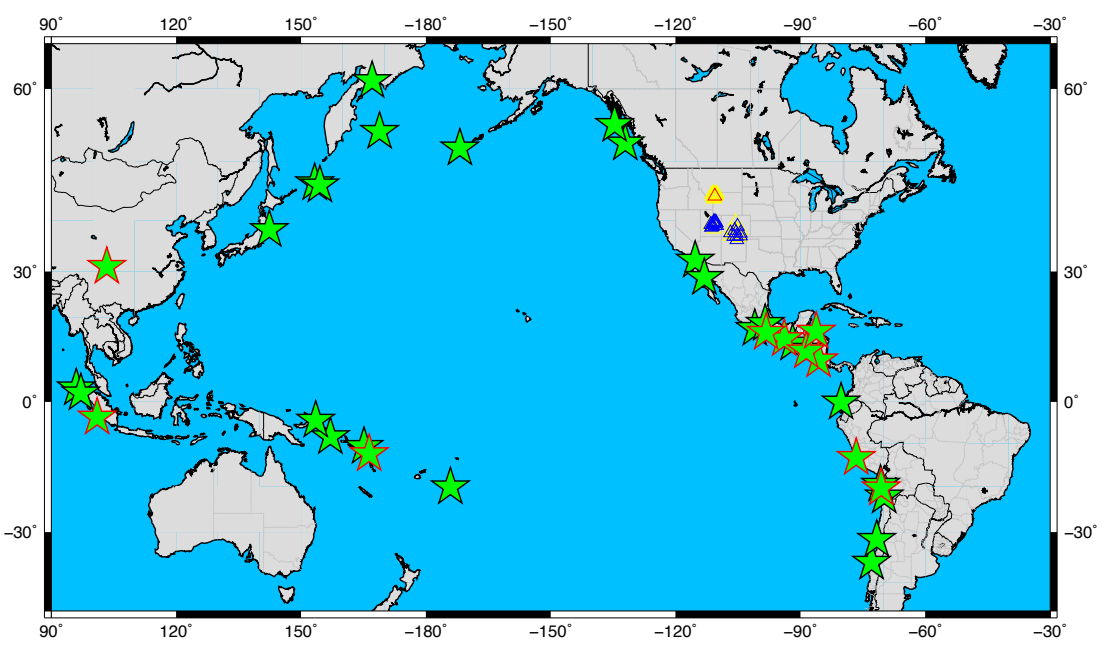
90°
120°
150°
−180°
−150°
−120°
−90°
−60°
−30°
60°
30°
0°
−30°

Figure 5.

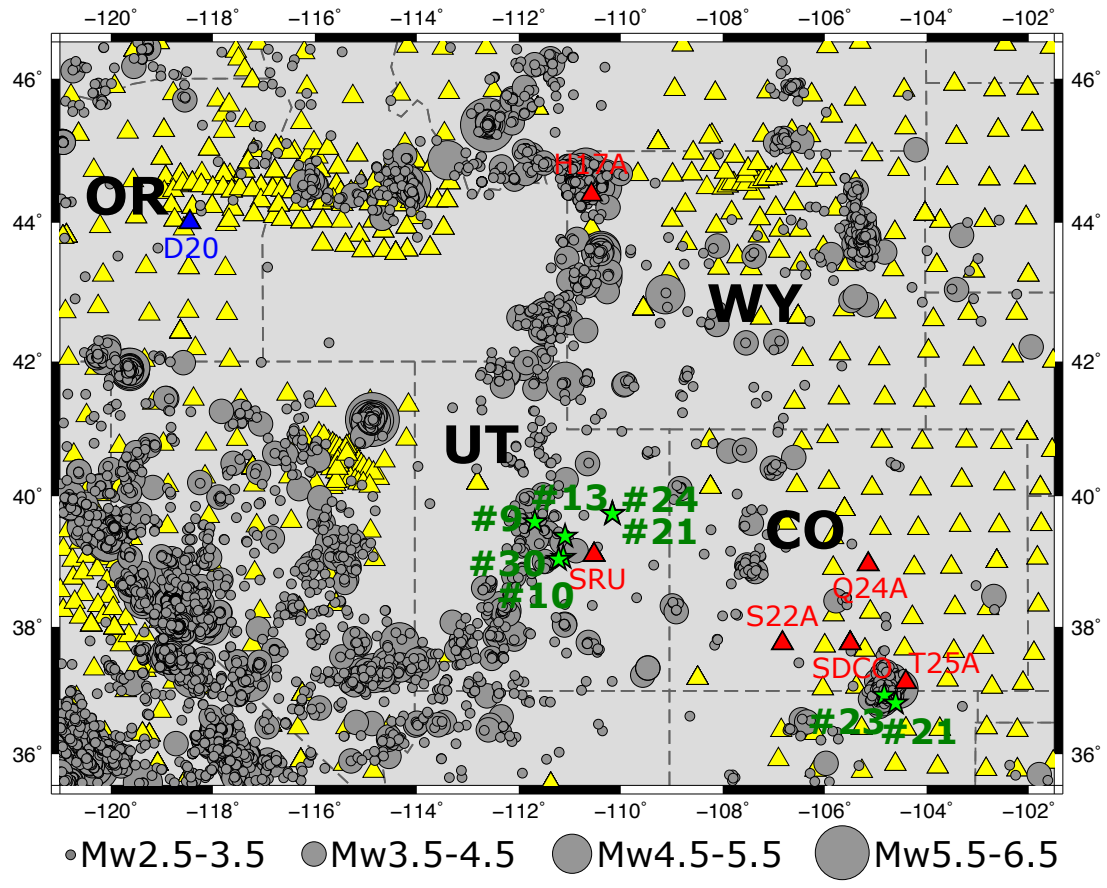
−120°
−118°
−116°
−114°
−112°
−110°
−108°
−106°
−104°
−102°
46°
44°
42°
40°
38°
36°
OR
D20
H17A
WY
UT
#13
#24
#9
#21
#30
SRU
#10
CO
Q24A
S22A
SDCO
T25A
#23
#21
Mw2.5-3.5
Mw3.5-4.5
Mw4.5-5.5
Mw5.5-6.5

Figure 6.

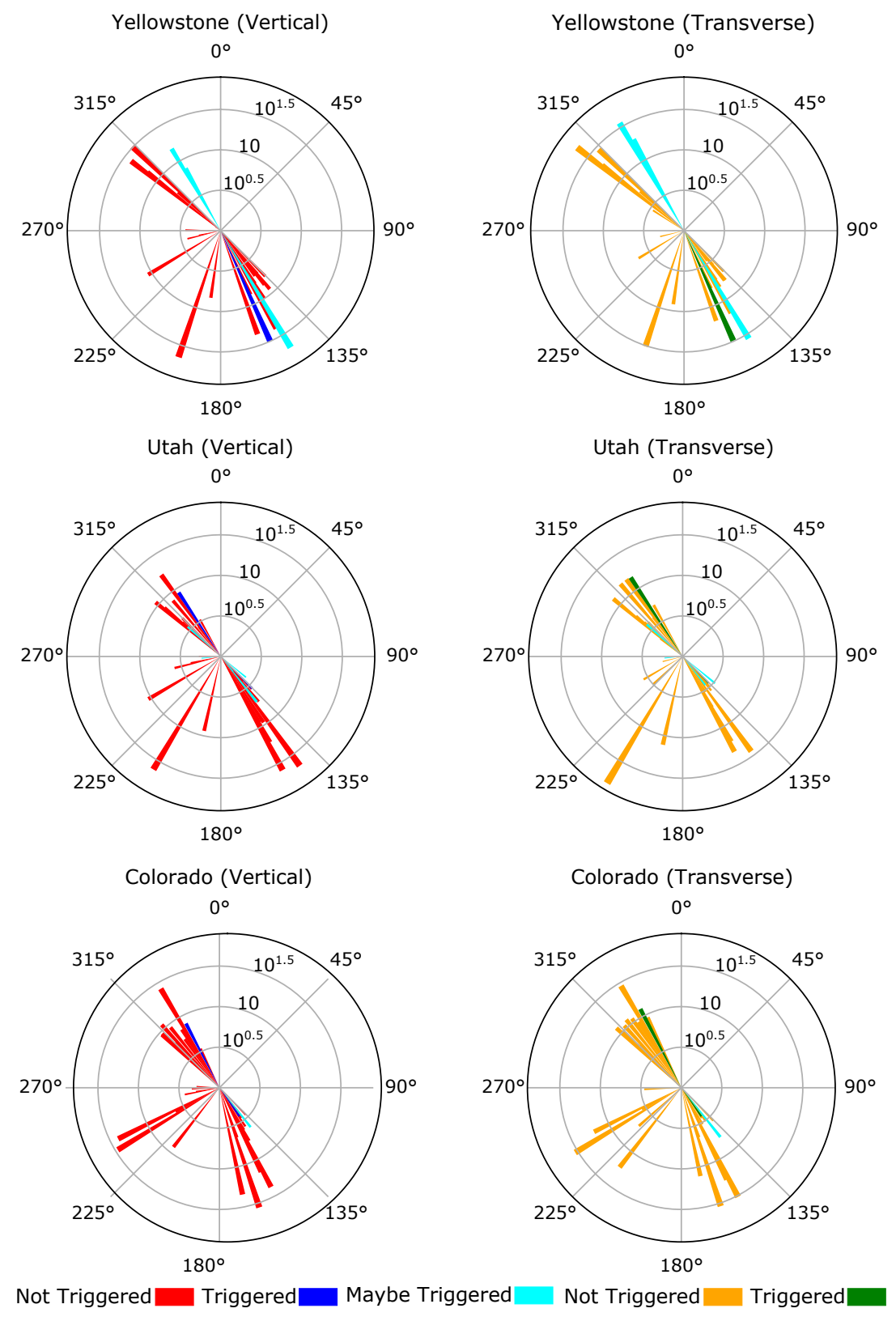
Yellowstone (Vertical)
Yellowstone (Transverse)
Utah (Vertical)
Utah (Transverse)
Colorado (Vertical)
Colorado (Transverse)
0°
45°
90°
135°
180°
225°
270°
315°
$10^{1.5}$
10
$10^{0.5}$
Not Triggered
Triggered
Maybe Triggered
Not Triggered
Triggered

Figure 7.

quake#21

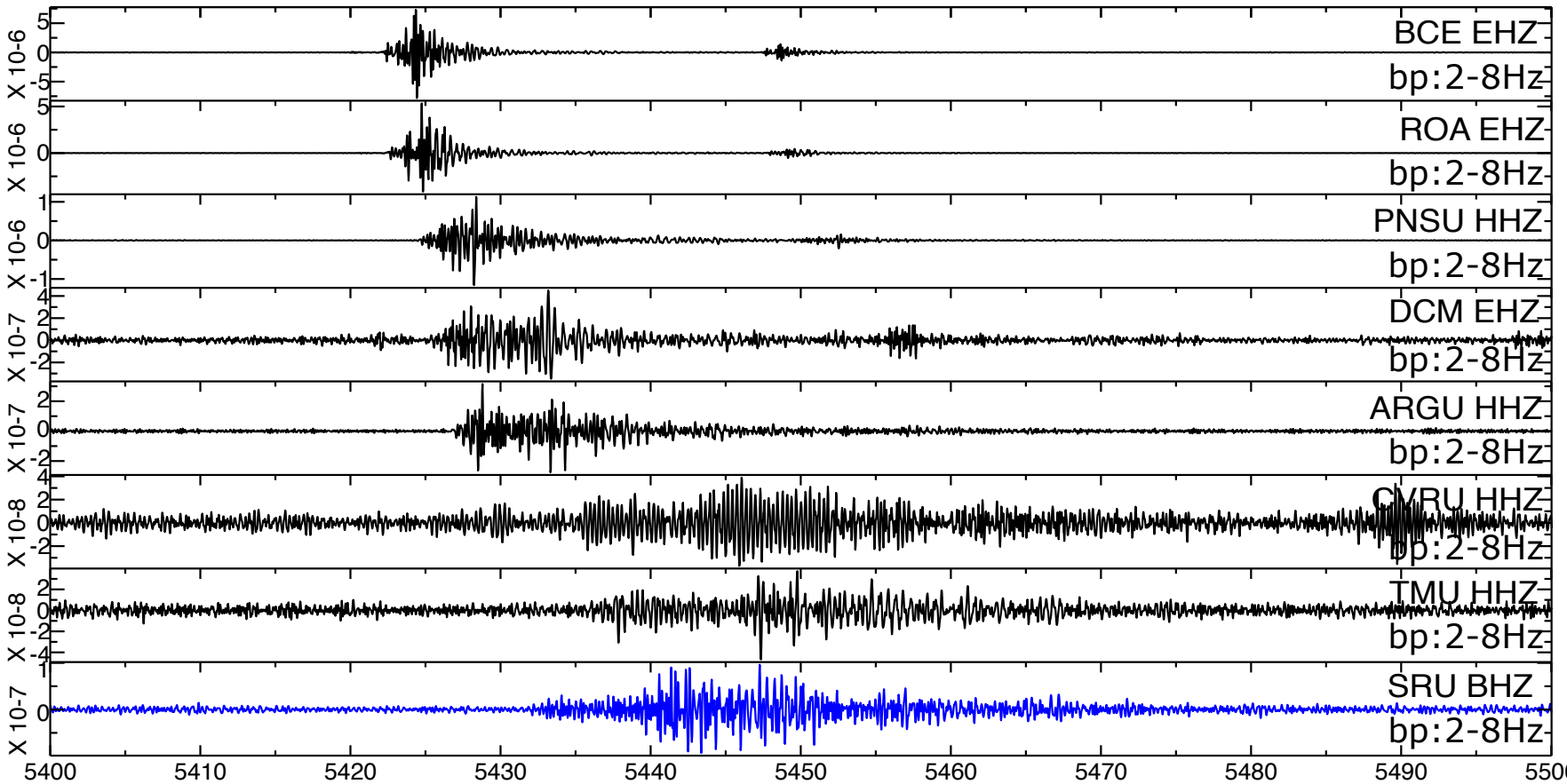
BCE EHZ
bp:2-8Hz
ROA EHZ
bp:2-8Hz
PNSU HHZ
bp:2-8Hz
DCM EHZ
bp:2-8Hz
ARGU HHZ
bp:2-8Hz
CMRU HHZ
bp:2-8Hz
TMU HHZ
bp:2-8Hz
SRU BHZ
bp:2-8Hz
X 10-6
X 10-7
X 10-8
5400
5410
5420
5430
5440
5450
5460
5470
5480
5490
5500

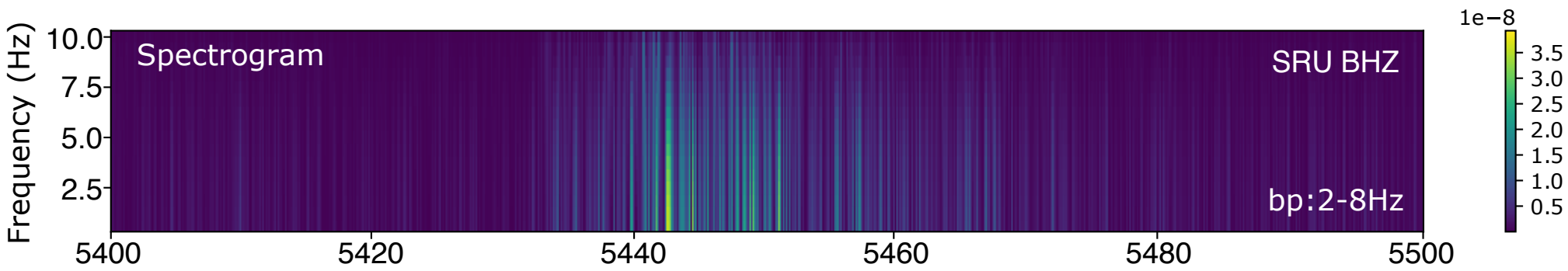
Spectrogram
SRU BHZ
bp:2-8Hz
Frequency (Hz)
10.0
7.5
5.0
2.5
1e−8
3.5
3.0
2.5
2.0
1.5
1.0
0.5
5400
5420
5440
5460
5480
5500

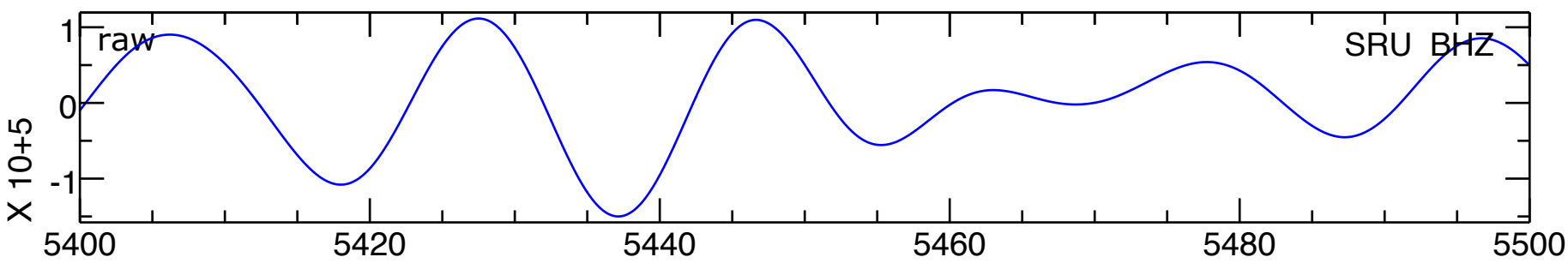
raw
SRU BHZ
X 10+5
1
0
-1
5400
5420
5440
5460
5480
5500

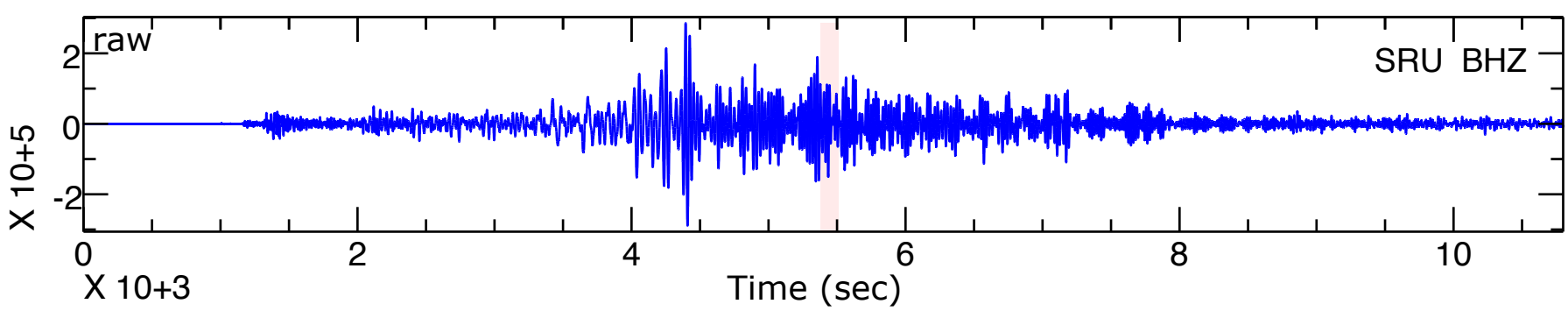
raw
SRU BHZ
X 10+5
2
0
-2
0
2
4
6
8
10
X 10+3
Time (sec)

Figure 8.

quake#21

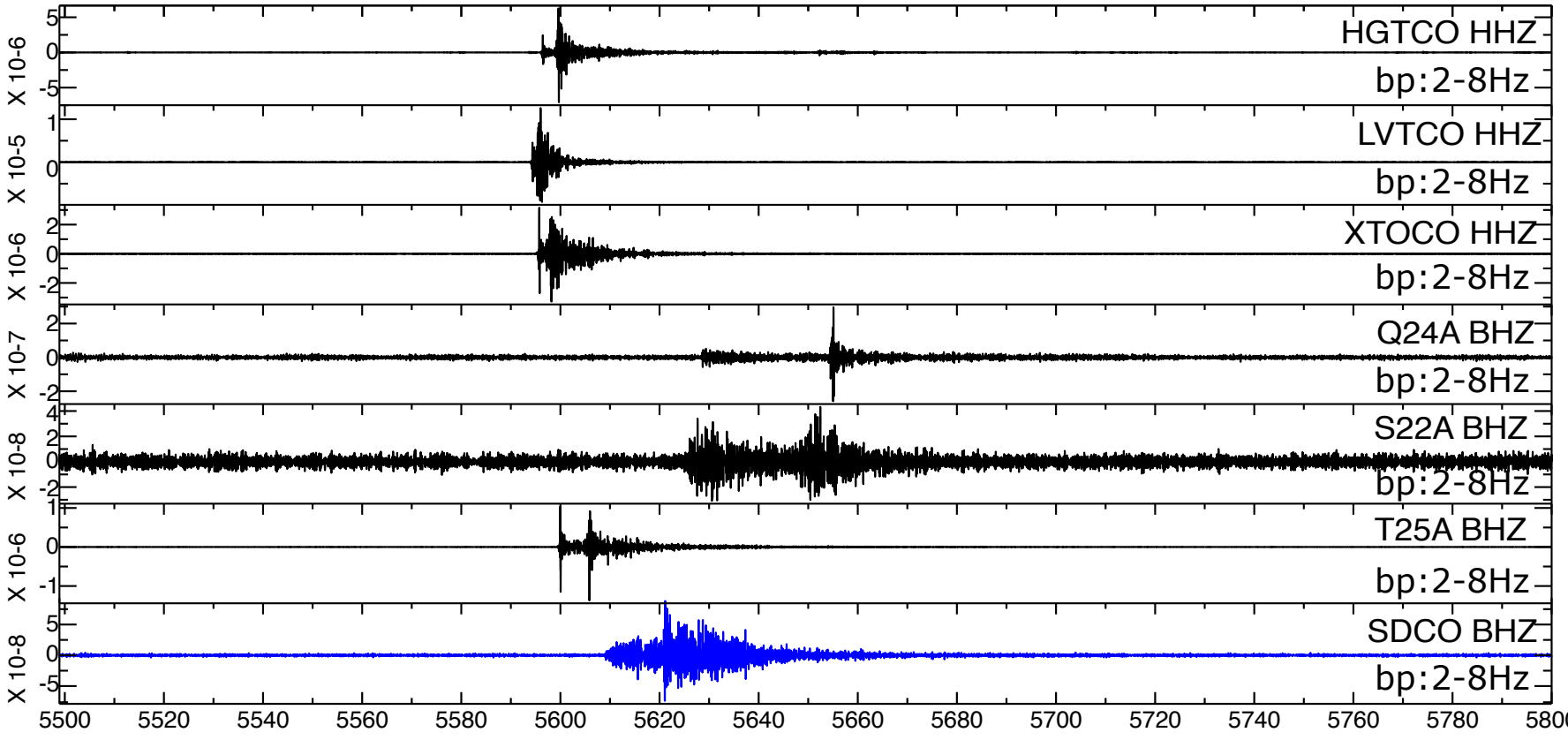
HGTCO HHZ
bp:2-8Hz
LVTCO HHZ
bp:2-8Hz
XTOCO HHZ
bp:2-8Hz
Q24A BHZ
bp:2-8Hz
S22A BHZ
bp:2-8Hz
T25A BHZ
bp:2-8Hz
SDCO BHZ
bp:2-8Hz
X 10-6
X 10-5
X 10-7
X 10-8
5500 5520 5540 5560 5580 5600 5620 5640 5660 5680 5700 5720 5740 5760 5780 5800

Spectrogram
SDCO BHZ
bp:2-8Hz
Frequency (Hz)
10.0
7.5
5.0
2.5
1e−8
2.5
2.0
1.5
1.0
0.5
5500 5550 5600 5650 5700 5750 5800

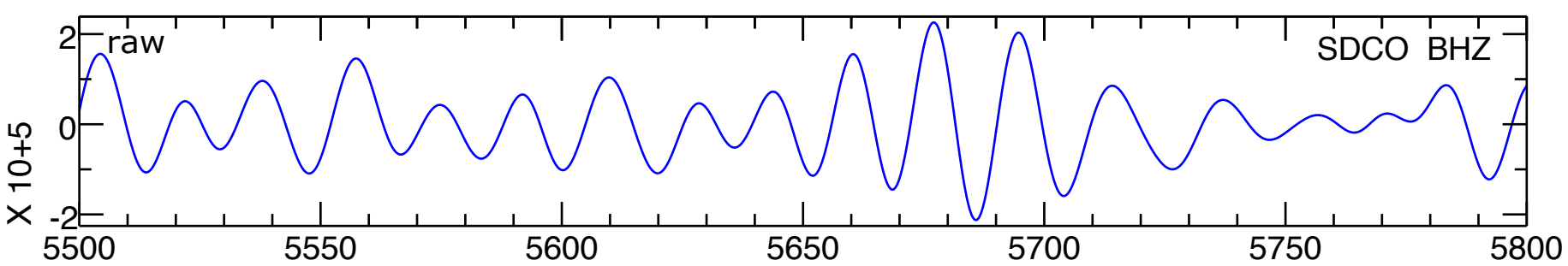
raw
SDCO BHZ
X 10+5
5500 5550 5600 5650 5700 5750 5800

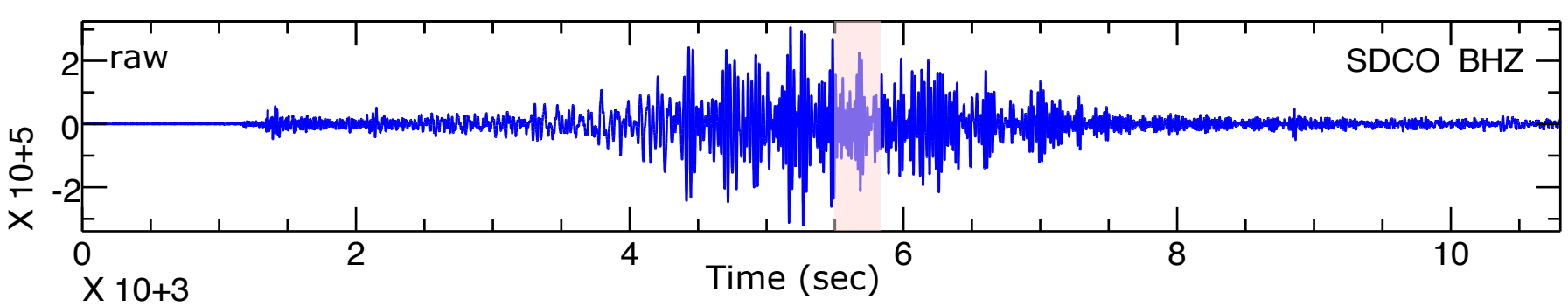
raw
SDCO BHZ
X 10+5
X 10+3
Time (sec)

Figure 9.

(a)

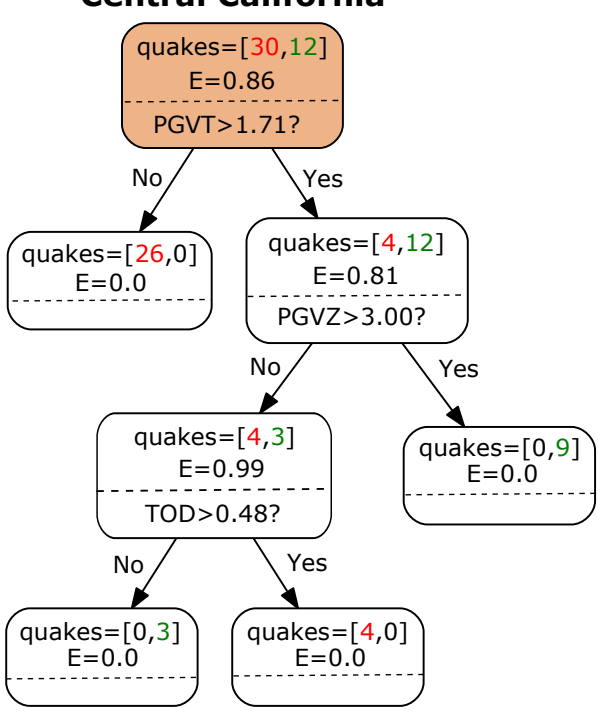
Central California
quakes=[30,12]
E=0.86
PGVT>1.71?
No
Yes
quakes=[26,0]
E=0.0
quakes=[4,12]
E=0.81
PGVZ>3.00?
No
Yes
quakes=[4,3]
E=0.99
TOD>0.48?
quakes=[0,9]
E=0.0
No
Yes
quakes=[0,3]
E=0.0
quakes=[4,0]
E=0.0

(b)

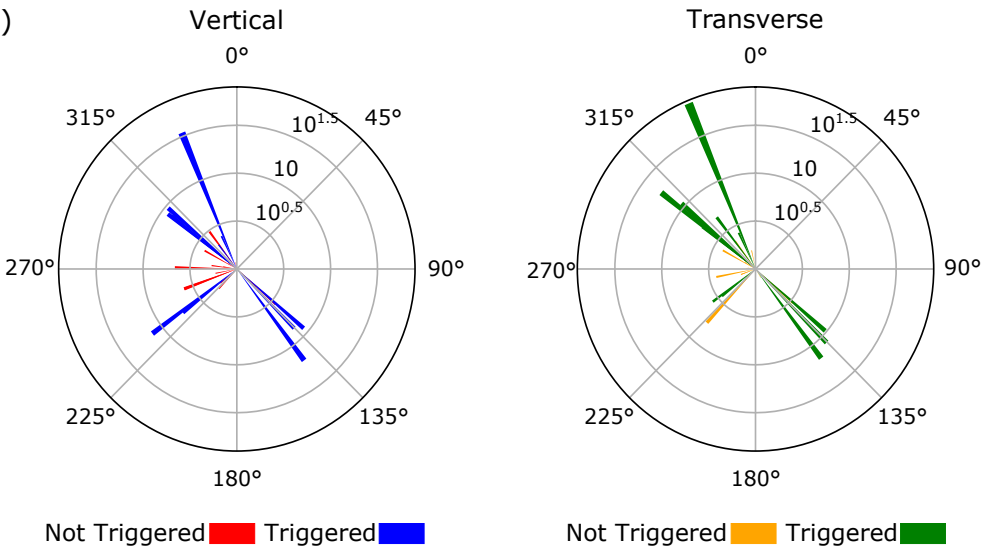
Vertical
0°
45°
90°
135°
180°
225°
270°
315°
$10^{1.5}$
10
$10^{0.5}$
Not Triggered
Triggered
Transverse
0°
45°
90°
135°
180°
225°
270°
315°
$10^{1.5}$
10
$10^{0.5}$
Not Triggered
Triggered

Figure 10.

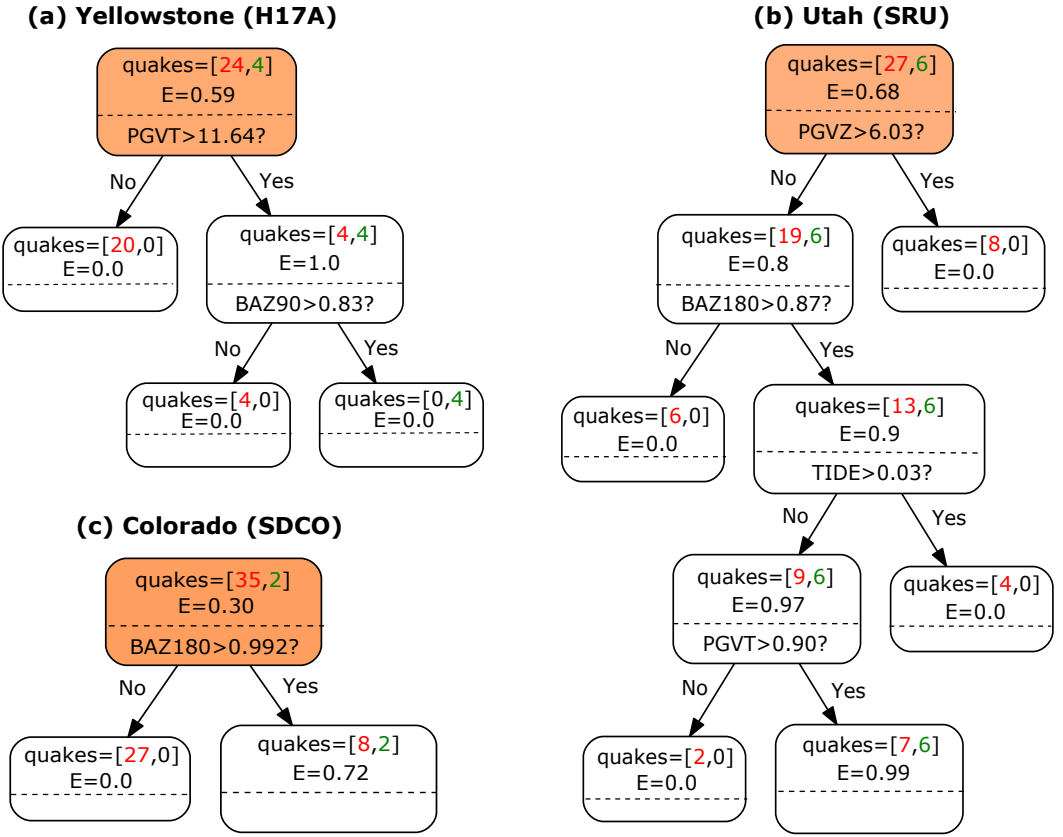
(a) Yellowstone (H17A)
quakes=[24,4]
E=0.59
PGVT>11.64?
No
Yes
quakes=[20,0]
E=0.0
quakes=[4,4]
E=1.0
BAZ90>0.83?
No
Yes
quakes=[4,0]
E=0.0
quakes=[0,4]
E=0.0
(b) Utah (SRU)
quakes=[27,6]
E=0.68
PGVZ>6.03?
No
Yes
quakes=[19,6]
E=0.8
BAZ180>0.87?
quakes=[8,0]
E=0.0
No
Yes
quakes=[6,0]
E=0.0
quakes=[13,6]
E=0.9
TIDE>0.03?
No
Yes
quakes=[9,6]
E=0.97
PGVT>0.90?
quakes=[4,0]
E=0.0
No
Yes
quakes=[2,0]
E=0.0
quakes=[7,6]
E=0.99
(c) Colorado (SDCO)
quakes=[35,2]
E=0.30
BAZ180>0.992?
No
Yes
quakes=[27,0]
E=0.0
quakes=[8,2]
E=0.72

Table 1.

Origin times and hypocenters of 38 earthquakes with M_w >= 7.0, along with whether their surface waves potentially triggered tremor in Yellowstone (H17A) or local earthquakes in central Utah (SRU) or the Raton Basin (SDCO). Yes: a local triggered event was identified; Maybe: a potentially triggered event was identified; **Yes/Maybe** (bold): this label was used in the decision tree algorithm; x: no events were identified; N/A: no data available.

#	Date & origin time	Longitude (^{o})	Latitude (^{o})	Depth (km)	Mw	H17A tremor	SRU quake	SDCO quake
1.	2004/12/23 14:59:30.9	161.25	-49.91	27.5	8.1	N/A	x	x
2.	2004/12/26 01:01:09.0	94.26	3.09	28.6	9.0	N/A	x	x
3.	2005/03/28 16:10:31.5	97.07	1.67	25.8	8.6	N/A	N/A	x
4.	2006/04/20 23:25:17.6	167.05	60.89	12.0	7.6	N/A	x	x
5.	2006/05/03 15:27:03.7	-173.47	-20.39	67.8	8.0	N/A	N/A	x
6.	2006/11/15 11:15:08.0	154.33	46.71	13.5	8.3	N/A	x	x
7.	2007/01/13 04:23:48.1	154.8	46.17	12.0	8.1	N/A	x	x
8.	2007/04/01	156.34	-7.79	14.1	8.1	N/A	Maybe	x

	20:40:38.9							
9.	**2007/08/15 23:41:57.9**	**-77.04**	**-13.73**	**33.8**	**8.0**	N/A	**Maybe**	x
10.	**2007/09/12 11:11:15.6**	**100.99**	**-3.78**	**24.4**	**8.5**	N/A	**Maybe**	x
11.	2007/11/14 15:41:11.2	-70.62	-22.64	37.6	7.7	x	x	x
12.	**2008/05/12 06:28:40.4**	**104.10**	**31.44**	**12.8**	**7.9**	**Maybe**	x	x
13.	**2009/05/28 08:25:04.8**	**-87.17**	**16.5**	**29.0**	**7.3**	x	**Maybe**	x
14.	2009/09/29 17:48:26.8	-171.97	-15.13	18.5	8.1	x	x	x
15.	2009/10/07 22:19:15.3	166.01	-11.86	41.7	7.8	x	x	x
16.	2010/02/27 06:34:13.0	-72.93	-36.15	28.1	8.8	x	x	x
17.	2010/04/04 22:41:09.2	-115.39	32.31	12.8	7.2	x	x	x
18.	2011/03/11 05:47:32.8	143.05	37.52	20.0	9.1	x	x	x
19.	2011/06/24 03:09:51.5	-171.77	52.09	74.2	7.3	x	x	x

20.	**2012/03/20 18:02:54.9**	**-98.39**	**16.6**	**15.4**	**7.5**	**Yes**	x	x
21.	**2012/04/11 08:39:31.4**	**92.82**	**2.35**	**45.6**	**8.6**	**Maybe**	**Yes**	**Yes**
22.	2012/04/12 07:16:04.6	-112.76	28.57	15.8	7.0	x	x	x
23.	**2012/08/27 04:34:39.5**	**-89.17**	**12.02**	**12.0**	**7.3**	x	x	**Yes**
24.	**2012/09/05 14:42:23.3**	**-85.64**	**10.00**	**29.7**	**7.6**	x	**Yes**	Yes
25.	2012/10/28 03:04:37.2	-132.06	52.61	12.0	7.8	x	x	x
26.	2012/11/07 16:35:56.3	-92.43	14.11	21.3	7.4	x	x	x
27.	2013/01/05 08:58:31.5	-134.97	55.69	13.8	7.5	x	N/A	x
28.	2013/02/06 01:12:55.0	165.21	-11.18	20.2	7.9	x	x	x
29.	2014/04/01 23:47:31.5	-70.81	-19.70	21.6	8.1	x	x	x
30.	**2014/04/03 02:43:35.9**	**-70.6**	**-20.43**	**28.7**	**7.7**	x	**Maybe**	x
31.	2014/04/18	-101.25	17.55	18.9	7.3	x	N/A	x

	14:27:36.0							
32.	2014/10/14 03:51:43.7	-88.45	12.33	40.8	7.3	x	x	x
33.	2015/09/16 22:55:22.9	-72.09	-31.13	17.4	8.3	x	x	x
34.	2016/04/16 23:58:57.0	-80.25	-0.12	22.3	7.8	x	x	x
35.	2016/12/17 10:51:56.3	153.76	-5.55	52.8	7.9	x	x	x
36.	2017/07/17 23:34:57.7	169.78	54.13	23.2	7.7	x	x	x
37.	**2017/09/08 04:49:44.2**	**-94.62**	**15.34**	**50.2**	**8.2**	**Maybe**	x	x
38.	2017/09/19 18:14:47.1	-98.62	18.51	52.7	7.1	x	x	x

Table 2. List of names of nearby station (right column) that recorded tremor in the Yellowstone region that was potentially triggered by some of the earthquakes from Table 1 (left column).

#	Date & origin time	Stations
12.	2008/05/12 06:28:40.4	H17A
20.	2012/03/20 18:02:54.9	H17A
21.	2012/04/11 08:39:31.4	H17A

37.	2017/09/08 04:49:44.2	H17A

Table 3. List of names of nearby station (right column) that recorded local earthquakes in central Utah that was potentially triggered by some of the earthquakes from Table 1 (left column).

#	Date & origin time	Stations
8.	2007/04/01 20:40:38.9	SRU
9.	2007/08/15 23:41:57.9	SRU, P14A, Q14A, P16A, Q16A, P17A, R17A, Q18A
10.	2007/09/12 11:11:15.6	SRU, TMU, Q18A, Q16A, P18A, ROA, P17A, DBD
13.	2009/05/28 08:25:04.8	SRU, Q16A, P18A, S18A, P19A, O19A, DUG, Q20A, R20A, O20A, S20A, N20A, N21A, N22A, R24A
21.	2012/04/11 08:39:31.4	SRU, TMU, CVRU, BCE, PNSU, ROA, DCM, ARGU
24.	2012/09/05 14:42:23.3	SRU, ARGU, DCM, PNSU
30.	2014/04/03 02:43:35.9	SRU, ARGU, CVRU, BCE, ROA, BCW, DCM, TMU, EMU, SNO

Table 4. List of names of nearby station (right column) that recorded local earthquakes in the Raton Basin, Colorado, that was potentially triggered by some of the earthquakes from Table 1 (left column).

#	Date & origin time	Stations
21.	2012/04/11 08:39:31.4	SDCO, T25A, Q24A, S22A, XTOCO, HGTCO, LVTCO

23.	2012/08/27 04:34:39.5	SDCO, T25A, S22A, Q24A, ANMO, TASL, TASM, KSCO, MVCO, ISCO, AMTX, MSTX, CBKS, OGNE, MNTX, WMOK
24.	2012/09/05 14:42:23.3	SDCO